Faculdade de Engenharia da Universidade do Porto
Instituto de Ciências Biomédicas Abel Salazar

Characterization of a collagen/nanohydroxyapatite scaffold for bone regeneration

Maria João Caspurro Vilela

Dissertation for the Master Degree in Bioengineering – Molecular Biotechnology

Supervisor: Christiane Salgado (PhD)
Co-supervisor: Fernando Jorge Monteiro (PhD)

October, 2019

"Pour ce qui est de l'avenir,
il ne s'agit pas de le prévoir
mais de le rendre possible."
Antoine de Saint-Exupéry

Abstract

Bone is a natural composite constituted by hydroxyapatite crystals, collagen, other non-collagenous proteins and cells. The presence of a mineralized matrix leads to a tougher composition of the tissue as well as allowing some of its functions, due to its mechanical properties.

Critical bone defects are very common and solutions for them need to be found in order to fill the space left and mimic the lost extracellular matrix. The most common solution is the use of autologous bone grafts, although they bring many disadvantages, like the risk of infection, higher morbidity associated to the donor tissue area and high costs. Therefore, it is important to find alternatives such as the use of biomimetic scaffolds, which need to be biocompatible, porous and allow cellular adhesion and proliferation, as well as diffusion of nutrients and oxygen. Natural or synthetic, hydrophilic polymeric solutions undergo freeze/thaw cycles, giving rise to a macroporous network that will allow cells migration, tissue ingrowth and the exchange of nutrients and other substances (e.g. hormones, cytokines and waste products) between the matrix and the cells. One example of a popular and promising polymeric scaffold are cryogels.

In this dissertation cryogels of collagen/nanohydroxyapatite were produced to be used in clinic for bone regeneration. They were characterized through physical, chemical, mechanical and biological studies, before and after sterilization by gamma irradiation. This sterilization, which is necessary in order for the materials to be used as medical devices in orthopaedics, showed no major modifications on the scaffolds behaviour, both physically and chemically. Swelling tests and dynamic mechanical analysis (DMA) were performed and showed an ability of the scaffolds to capture and retain solvents as well as adequate mechanical resistance and viscoelastic properties. Through Scanning Electron Microscopy (SEM), it was possible to observe that the materials had a heteroporous morphology with microporosity and macroporosity, important parameters to promote bone regeneration. Using Fourier Transform Infrared spectroscopy (FT-IR) the collagen/nanohydroxyapatite composition of the scaffolds was confirmed. For the biological studies, metabolic activity assays were performed and showed no evidence of cytotoxicity of the cryogels when

in contact with fibroblasts (L929) and osteoblast-like cells (MG63). Additionally, after 14 and 21 days of incubation with the materials, a study of the alkaline phosphatase (ALP) activity, a DNA quantification and an analysis through Confocal Laser Scanning Microscopy (CLSM) were performed. The results showed that the scaffolds promoted the proliferation of the cells and the expression of the osteoblastic phenotype.

Keywords: Cryogel, bone regeneration, scaffold, collagen, nanohydroxyapatite

Acknowledgements

First of all, I would like to thank my supervisor, Dr. Christiane Salgado, for all the guidance throughout these two years, for sharing all her knowledge with me and for being available to answer the tiniest doubts. I learned a lot from her. I will take all her teachings with me for the future and will always remember her as a role model.

I would also like to thank my co-supervisor, Prof. Fernando Jorge Monteiro for giving me the chance to take part in this amazing project and contribute to the evolution of science and medicine. You are a true example of professionalism and dedication.

I am very grateful to the company "Artur Salgado S.A" for their collaboration during this project and for giving me the opportunity to combine lab work with the industrial sector.

To my group, Biocomposites, thank you for all the fun and relaxing moments and for always being there for me when I needed. To all the technicians and researchers that helped me during my time in i3S, a special thanks to you too.

To my parents and sisters, you were my rock during all these years. Thank you for all the support, hugs and love. To my grandparents, thank you for your friendship and inspiration. I hope that you are proud of my path.

To my boyfriend, André, thank you for your love and companionship, for knowing how to motivate me, for always making me laugh and for all the experiences. To my best friend, Inês Rocha, my forever chromosome, thank you for all the fun moments, the everlasting memories and the unconditional support. To all my closest friends, Inês Guimarães, Catarina Pinto and Valéria Rocha, thank you for your friendship and trust.

To finish, I would like to show a special appreciation for BEST Porto and its members. You showed me what team-work and companionship mean and you were truly the BEST part of my academical years.

Table of contents

List of figures

List of tables

List of abbreviations and symbols

List of abbreviations

2D	Two-dimensional
3D	Three-dimensional
ATR	Attenuated Total Reflectance
BMPs	Bone Morphogenic Proteins
BSA	Bovine Serum Albumine
CLSM	Confocal Laser Scanning Microscopy
Cw	Swelling equilibrium
CO_2	Carbon dioxide
DMA	Dynamic Mechanical Analysis
DMEM	Dulbecco's Modified Eagle Medium
ECM	Extracellular matrix
EDC	1-ethyl-3-(3-dimethyl aminopropyl) carbodiimide hydrochloride
FBS	Fetal Bovine Serum
FT-IR	Fourier Transformed Infrared
GAGs	Glycosaminoglycans
HA	Hydroxyapatite
HCl	Hydrochloric acid
NHS	N-hydroxysuccinimide
OPD	Optical Path Difference
OPG	Osteoprotegerin
PBS	Phosphate-buffered saline
SEM	Scanning Electron Microscopy
Wd	Materials' dry weight
Ws	Materials' swollen weight

List of symbols

Ø	Diameter

Chapter 1

Objective and Document Structure

1.1 Objective of the work

The present dissertation results from a collaboration between the "Biocomposites" group of INEB (Instituto de Engenharia Biomédica/i3S – Instituto de Investigação e Inovação em Saúde) and the company "Artur Salgado S.A", through project COLHYBRID.

The objective of this project is to perform and evaluate a scale-up production process of a porous scaffold based on collagen and nanohydroxyapatite, which promotes bone regeneration and works as a barrier for both fibrosis and proliferation of scar tissue, considering all the experiments in the work previously developed by Sandra C. Rodrigues (C. et al., 2013).

The material was produced using a prototype bioreactor at the company development lab, for a larger scale production line, instead of a small scale production in the laboratory bench, in order to produce an appropriate medical device for the orthopaedic market. The production gave origin to porous membranes with two different sizes that were then analysed in the i3S facilities. Four batches of the material were studied before (A-D) and after (A'-D') sterilization through gamma irradiation (15 kGy).

The main tasks of the work included the physical, chemical, mechanical and biological characterization of the product. Fourier transform infrared spectroscopy (FT-IR) was used to observe if the different samples had the same

transmittance spectrum; confocal laser scanning microscopy (CLSM) was performed to observe the cell/materials surface interaction; images from scanning electron microscopy (SEM) were analysed to observe the materials surface and the morphology and size of the pores; swelling capacity test evaluated the ability of the cryogels to capture and retain water based solutions; compression cycles from a dynamic mechanical analysis (DMA) evaluated the mechanical properties of the material; MTT and Alamar blue assay with two different cell lines (L929-fibroblasts from mouse subcutaneous and adipose tissue and MG63-osteoblast-like cells from human bone osteosarcoma) measured the metabolic activity of the cells when in direct or indirect contact with the samples; early osteoblast differentiation (MG63) was observed by cellular alkaline phosphatase (ALP) activity; and cell proliferation profile was quantified by DNA concentration (PicoGreen assay).

1.2 Document structure

This dissertation is divided in 5 chapters. Chapter 1 presents the main goal and tasks of the work, while Chapter 2 includes the literature survey and state of art. In Chapter 3 there is a description of the methodology used for the mechanical, physical, chemical and biological characterization of the materials and Chapter 4 describes the results obtained and their subsequent discussion. The last chapter presents the conclusions of the work developed and gives a brief perspective for future work.

Chapter 2

Literature Review

2.1 Introduction

The extracellular matrix (ECM) is very important for cell's microenvironment and survival. It not only gives structural support to cells and tissues, but also provides signalling cues that regulate cells behaviours in multicellular organisms, such as cell growth, differentiation, shape and viability (Lukashev & Werb, 1998).

It is composed by structural proteins (i.e. collagen), polysaccharides/glycosaminoglycans (GAGs) and adhesion proteins, such as integrins, that make the connection between the ECM and the cells. These constituents are constantly being synthesized, secreted and exchanged between the cells and the ECM.

In bone, the extracellular matrix is a key part of the tissues' structure and function. It is more rigid than the ECM that is present in other tissues because of tissue mineralization, which is the deposition of calcium phosphate crystals, corresponding to the inorganic phase of bone (V. & Matthias, 2002).

Bone is a tissue that is in constant change, having high rates of formation and degradation. A slight dysregulation of these rates can lead to osteoporosis (formation of less bone) or osteopetrosis (formation of more bone), two conditions that can cause fracture of the bones and, consequently, the

appearance of critical-size defects (over 4 mm), which bones cannot self-regenerate (Boskey, 2008; Lazner, Gowen, Pavasovic, & Kola, 1999). Alternatives need to be found in order to produce bone tissue ingrowth into the critical defect. In addition to this, bone loss due to congenital defects, trauma, accident, infections or after tumour resection are major clinical problems that need to be addressed (Bran, Stern-Straeter, Hörmann, Riedel, & Goessler, 2008; Ruchi, Kumar, Chand, & Ashok, 2014).

The use of autologous bone grafts is the most common procedure to treat these clinical problems, though there is the possibility of infection and implant rejection, as well as of donor site morbidity. Also, they are associated with high costs (Bran et al., 2008; K. R. Hixon, C. T. Eberlin, et al., 2017). To try to avoid these major disadvantages, alternatives need to be found and that is where materials that are able to mimic the mechanical properties, structure and functions of the bone tissue appear (Shakya & Kandalam, 2017).

Previous studies have demonstrated that cells behave differently in two-dimensional (2D) and three-dimensional (3D) cultures. 3D cell cultures are more similar to *in vivo systems*, so they should be preferably used. In 3D structures, it is possible to see the whole structure of the ECM as well as the interactions between the matrix and the cells (Stevens & George, 2005; Tian et al., 2008). With that information, 3D scaffolds are widely used in bone regeneration to promote tissue growth by mimicking the ECM of the native tissues (Inzana et al., 2014; Jones, Gentleman, & Polak, 2007; Petite et al., 2000).

Ideal scaffolds should be biocompatible, biodegradable and no immunogenic, promote cell and materials surface interactions to allow adhesion, provide the dispersion of nutrients and other molecules through its structure and have suitable mechanical properties, depending on their final application. Thus, an adequate biomaterial for bone regeneration application needs to be osteoinductive, osteoconductive and osteogenic (K. R. Hixon et al., 2016).

3D scaffolds can have different shapes and sizes, different fabrication techniques and different composition. Nowadays, some of the most common scaffolds are electrospun fibbers, decellularized tissues, microspheres, ceramics, hydrogels and cryogels. This last form of scaffold, with a composition of collagen and nanohydroxyapatite similar to the bone, was the one chosen in our work to be used as a medical device in bone regeneration. Our material is characterized by a more heterogenous porosity than in the natural bone tissue,

which varies according to the location, size and type of bone. That large profile of pore size allows the use of the studied material into different bone defects. The scaffolds' mechanical properties showed similar characteristics to the native bone ECM which is an advantage for its application as a medical device in bone regeneration.

2.2 Bone

Bones are natural composites that can have many functions like the support of soft tissues, movement and anchoring of the muscles, mechanical protection of the inner organs such as the brain and the lungs, the production of blood cells, because they contain the bone marrow, and the storage of minerals, growth factors and cytokines (Seeley, Stephens, & Tate, 2002).

As we can see in Figure 1, the bone structure can be divided into 5 main levels.

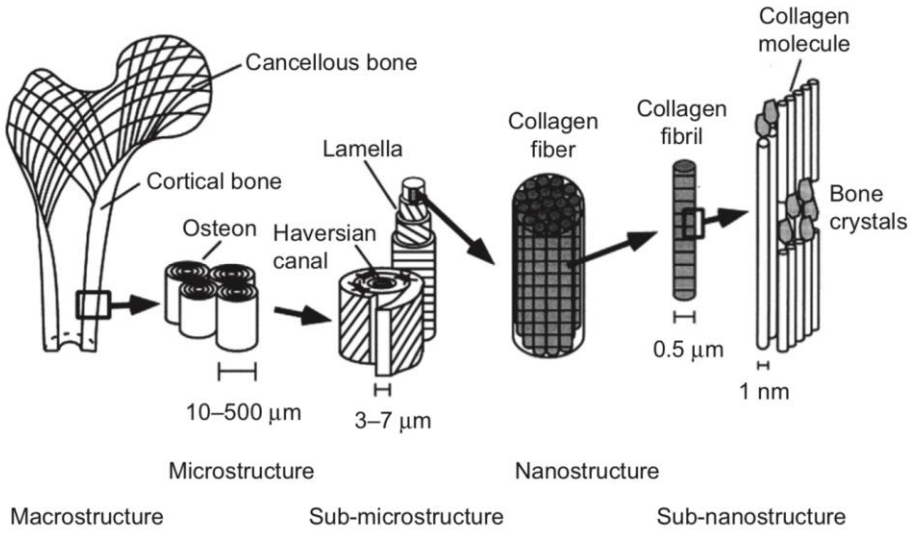

Figure 1 - Structure of the bone in different scales (Rho, Kuhn-Spearing, & Zioupos, 1998).

At the macrostructural level, bone can be of 2 types. One of them is the compact/cortical bone which represents 80% of the skeleton and in which it is possible to find tunnels with blood vessels and nervous fibbers. The other type

is the trabecular/cancellous bone, which corresponds to the remaining 20% of the skeleton, is more porous and is where we find the bone marrow (Ott, 2018). Cortical bone is found at the outer part of bones, whereas cancellous bone is located at their inner part. Cortical bone is surrounded by a membrane of fibrous tissue called periosteum and separated from cancellous bone by the endeosteum (Clarke, 2008). At the microscopic level, we have the trabecula and the osteon, which are the basic units of cancellous and cortical bone, respectively. The osteon is composed by a Haversian canal, through which nerves and blood vessels pass, and is surrounded by lamella in the shape of a cylinder. At the sub-microscopic level, both cortical and cancellous bone are composed by lamella. At the nanostructural scale it is possible to find the collagen fibers and the minerals around them. Finally, at the sub-nanostructural level there are the molecules of collagen, the minerals and the other non-collagenous proteins (Jiang & Liu, 2016).

The composition of this tissue has 2 phases: an inorganic one and an organic one.

The inorganic phase is mainly constituted by apatite that perform as regulator of calcium levels through the remodelling (degradation/formation) of bone (Muschler, Raut, Patterson, Wenke, & Hollinger, 2010). This process has to be carefully controlled because a lack of calcium will lead to muscular, cardiac and renal problems. The inorganic phase is also responsible for assuring the levels of phosphorus in the organism.

The organic phase is formed by collagen type I, other proteins and cells which are responsible for the formation and degradation of the tissue and are represented in figure 2.

On the side of the bone producer cells we can find mesenchymal stem cells and osteoblasts (and & Wagner, 1998). These last ones have origin in mesenchymal stem cells and can be found on the surface of the bone, forming and mineralizing the ECM, or inside the ECM, where they maturate and originate osteocytes. The differentiation of osteoblasts depends on the presence of both the transcription factor Runx2 and bone morphogenic proteins (BMPs) (Walsh, 2015). Osteocytes are the cells present in majority (90% of the total bone cells) and either are responsible for bone maintenance or enter a senescence phase, becoming bone lining cells, which protect the non-active surfaces of the bone. Bone's formation has a duration of 4 to 6 months.

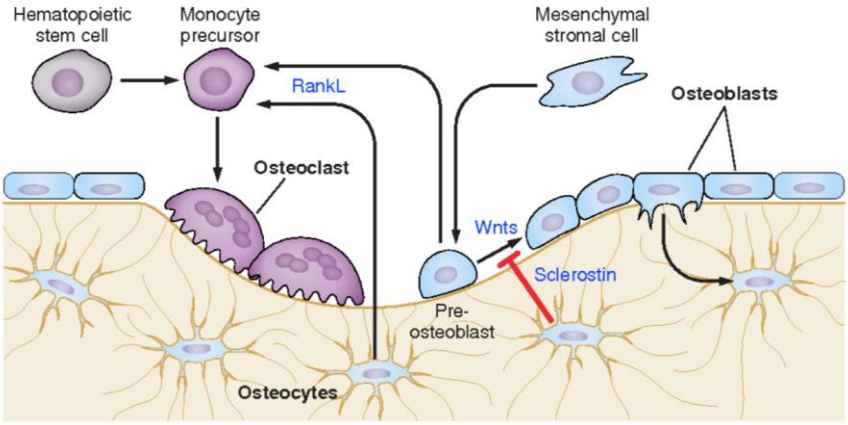

Figure 2 - Bone cells (Riddle & Clemens, 2017).

The bone degrading cells are osteoclasts derived from the monocyte lineage and they destroy bone through acidification of the medium by the secretion of enzymes and hydrogen ions. Osteoclasts life cycle is regulated by RANKL, which is the receptor activator of NF-kB ligand, and osteoprotegerin (OPG) (Clarke, 2008). Bone's degradation takes approximately 2 to 4 weeks.

Bone remodelling can be controlled by hormones, cytokines, growth factors, physical activity associated with mechanical forces and neuropeptides/neurotransmitters.

The equilibrium between bone producing cells and bone degrading cells is extremely important and sensitive and any change can lead to diseases, like osteoporosis. Also, cysts or tumour resection and fractures could give rise to non self-healing defects (critical size defects).

2.3 Cryogels

Cryogels are nowadays seen as novel and important scaffolds for bone regeneration, being an alternative to some of the other methods used for this kind of regeneration, such as bone grafts and hydrogels (Bencherif et al., 2012).

In cryogels synthesis, the gel precursors, more specifically hydrophilic

polymer chains, are cross-linked and subsequently frozen. The crosslinking can be achieved physically or chemically. The water in the polymeric solution will freeze, forming ice crystals. As it sets, the surrounding gel will become increasingly more concentrated. The critical stage of the cryogel fabrication occurs in the frozen state, where the chemical reaction of polymerization occurs. During this period, the gelation rate, time and temperature will have a crucial role in the structure of the cryogel, such as the material porosity. The temperatures usually vary between -5ºC and -20ºC and slower freezing rates result in larger pores with increased interconnectivity. The opposite will happen with faster rates. After the freezing step, the cryogel can thaw at room temperature, during which melting of the crystals occurs, leading to the characteristic macroporous network structure (Fig. 3) (K. R. Hixon, Lu, & Sell, 2017; Shakya & Kandalam, 2017). This production process is easy and fast. The macroporosity will allow angiogenesis, rapid swelling (they can hold up to 99% of water) and cell infiltration in the structure. The cryogel will also have a sponge-like behaviour, be mechanically stable, have mechanical properties similar to native cell tissue ECM and be biocompatible and degradable (Katherine R Hixon, Melvin, Lin, Hall, & Sell, 2017).

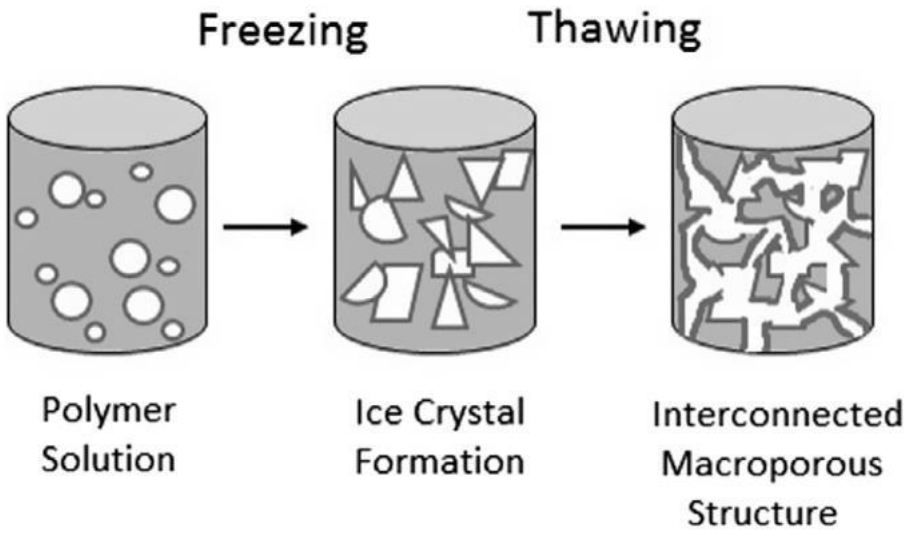

Figure 3 - Steps of formation of cryogels, resulting in an interconnected and macroporous structure (K. R. Hixon, T. Lu, et al., 2017).

The properties of the cryogels should be adjusted to the tissues application and could be modified by changing the polymer concentration, the

temperature of manufacturing, freezing rates and thawing rates.

Cryogels can have many applications such as cancer vaccines, 3D models, cosmetics, medical devices, agriculture, drugs and cells delivery systems, bioreactor systems, cell separation and in tissue engineering.

In the biomedical field, cryogels applications are in tissue regeneration, more specifically for bone tissue (Razavi, Qiao, & Thakor, 2019).

Table 1 - Natural and synthetic polymers commonly used in the fabrication of cryogels for bone tissue applications.

Source	Polymer
Natural	Alginate-Agarose
	Chitosan
	Gelatine
	Chitosan-Gelatine
	Collagen
	Silk fibroin (SF)
Synthetic	N-vinyl-2-pyrrolidone (NVP)
	Poly(ethylene oxide) (PEO)

As we can see in Table 1, there are various polymers that can be used to develop cryogels as a tissue engineering scaffold for bone defects. Some of these materials can also be used in other biomedical applications for different tissues rather than bone and in other combinations.

These polymers can have two sources: natural or synthetic. It is also possible to combine these two and have biosynthetic polymers.

A natural polymer has its origin in living organisms, such as plants and animals, whereas synthetic polymers are produced artificially (Alina Sionkowska, 2011). Natural polymers have been winning increasingly more importance in the biomedical field due to their high biocompatibility although their costs are still higher than the ones associated with synthetic polymers.

In the next subchapter, collagen-hydroxyapatite cryogels for bone regeneration will be further described.

2.3.1 Collagen-hydroxyapatite cryogels

Collagen is a fibrillar structural protein and collagen type I is the major organic constituent of many tissues, including bone. It is formed by three polypeptide chains based in repetitions of the motif (Gly-X-Y), where X and Y are amino acids (Shoulders & Raines, 2009). It is a biocompatible, biodegradable and versatile material that can adjust its elasticity and toughness to the tissue where it stands through intermolecular cross-linking (Lee, Singla, & Lee, 2001). In fact, the collagen degree of organization reflects the tissue maturity.

Hydroxyapatite ($Ca_{10}(PO_4)_6(OH)_2$) is similar to the main mineral present in bone tissue, apatite, and is therefore a ceramic widely used as bone substitute due to its bioactivity, lack of cytotoxicity and its capacity to provide stiffness (Suchanek & Yoshimura, 1998). In order to better mimic bone, nanohydroxyapatite (nanoHA) may be used given its smaller size and huge specific surface area (Webster, Ergun, Doremus, Siegel, & Bizios, 2000).

In many studies of bone regeneration applications, collagen is combined with hydroxyapatite, in order to obtain a composite that is biocompatible, biodegradable and that mimics the mechanical properties of the tissue (C. et al., 2013; Du, Cui, Feng, Zhu, & de Groot, 1998; Laranjo, Liliana, Helena, Jorge, & Jorge, 2016; Raina et al., 2016; Suchanek & Yoshimura, 1998).

Some studies showed that collagen-nanohydroxyapatite cryogels had interconnected pores, good mechanical properties resembling a gel and increased osteoblast-like cell proliferation, which makes this scaffold a proper application for bone regeneration (C. et al., 2013). Compared to other scaffolds (Kane & Roeder, 2012; Kathuria, Tripathi, Kar, & Kumar, 2009; Yeong, Chua, Leong, Chandrasekaran, & Lee, 2007), these cryogels have biocompatibility and a heteroporous structure with good swelling rate in water solvents that does not compromise the mechanical properties.

In one of these studies the authors were able to identify the ideal

composition of the cryogels: 30% collagen and 70% of nanohydroxyapatite. Both *in vitro* and *in vivo* studies revealed HBMSC (human bone marrow stromal cells) differentiation in osteoblastic cells, low inflammatory response and an increase of angiogenesis in the defect site as well as bone tissue formation and biodegradation of the scaffold after 4 weeks of subcutaneous implantation (Laranjo et al., 2016).

The basis of this work were the studies carried out by Sandra C. Rodrigues (C. et al., 2013) and the cryogels produced had a composition of 50% collagen and 50% nanohydroxyapatite. The materials were then studied before and after being sterilized through gamma irradiation to evaluate their security and reproducibility. As a final application, the materials will be used as medical devices to fill bone defects. Unlike the most widely used medical devices in the orthopaedic sector, the prostheses, the studied material will not only mimic the bone ECM, but also the mechanical properties. This biodegradable material allows the bone cells ingrowth which favours its use as a bone regenerative scaffold. Regarding bone substitutes that already exist in the market (MedicalExpo, 2019), these are rigid and sold in specific sizes and shapes. In comparison, our materials are ductile and allow the orthopaedic surgeons to cut the material as desired to better fit in the critical size defect. Also, when in contact with the body fluids, the scaffold will expand and adapt to the defect.

Chapter 3

Materials and Methods

3.1 Materials

Type I collagen from bovine Achilles tendon, 3-(4,5-dimethyl-2-thiazolyl)-2,5-diphenyltetrazolium bromide (MTT), alamar blue dye (resazurin), magnesium chloride ($MgCl_2$), 4'-6-diamidine-2-phenylindole (DAPI), formaldehyde 4% and Triton X100 were purchased from Sigma-Aldrich (St. Louis, MO); Viscolma collagen suspension dissolved at 12% was purchased from Viscofan BioEngineering (Germany); 1-ethyl-3-(3-dimethyl aminopropyl) carbodiimide hydrochloride (EDC) and N-hydroxysuccinimide (NHS) were purchased from Fluka (Buchs, Switzerland). Hydrochloric acid (HCl) and dimethyl sulfoxide (DMSO) were obtained from Merck (Germany) and nanohydroxyapatite (nanoXIM) aggregates were kindly provided by Fluidinova S.A. (Maia, Portugal). Dulbecco's modified eagle medium (DMEM), fetal bovine serum (FBS), fungizone, penicillin-streptomycin and trypsin were purchased from Gibco (U.S.A.). DC™ protein assay was purchased from Bio-Rad. Alexa fluorconjugated phalloidin 594 and the Quant-iT™ Picogreen® DNA assay kit were purchased from Invitrogen (UK).

3.2 Preparation of the collagen-nanoHA scaffolds

For batches A-C, Achilles tendon bovine collagen type I (Sigma-Aldrich) was dissolved using a diluted solution of HCl (10 mM) and kept at 4°C. For batch D, a collagen solution (12%-Viscolma collagen suspension) was purchased from Viscofan BioEngineering. In order to remove all the lumps of the solutions, they were homogenized at 20.000 rpm (Ultra Turrax T25, IKA) at 4ºC for about 1 hour and 30 minutes. To produce the samples, the collagen solution was mixed using a peristaltic pump, first with a HCl and nanohydroxyapatite solution and after homogenization with a HCl, EDC (40 mM) and NHS (20 mM) solution. Collagen and nanoHA were in a 50:50 % wt proportion. The resultant solution fulfilled two sizes of glass molds (5 and 10 cm of diameter) and was kept in the freezer for 24 hours. Finally, samples were dried using a freeze-drier (Labconco) for 24 hours (-80ºC) and the resultant scaffolds can be observed in Figure 4. Some samples were submitted to sterilization through gamma irradiation (15 kGy). Four batches of the material were studied before (A-D) and after (A'-D') their gamma irradiation.

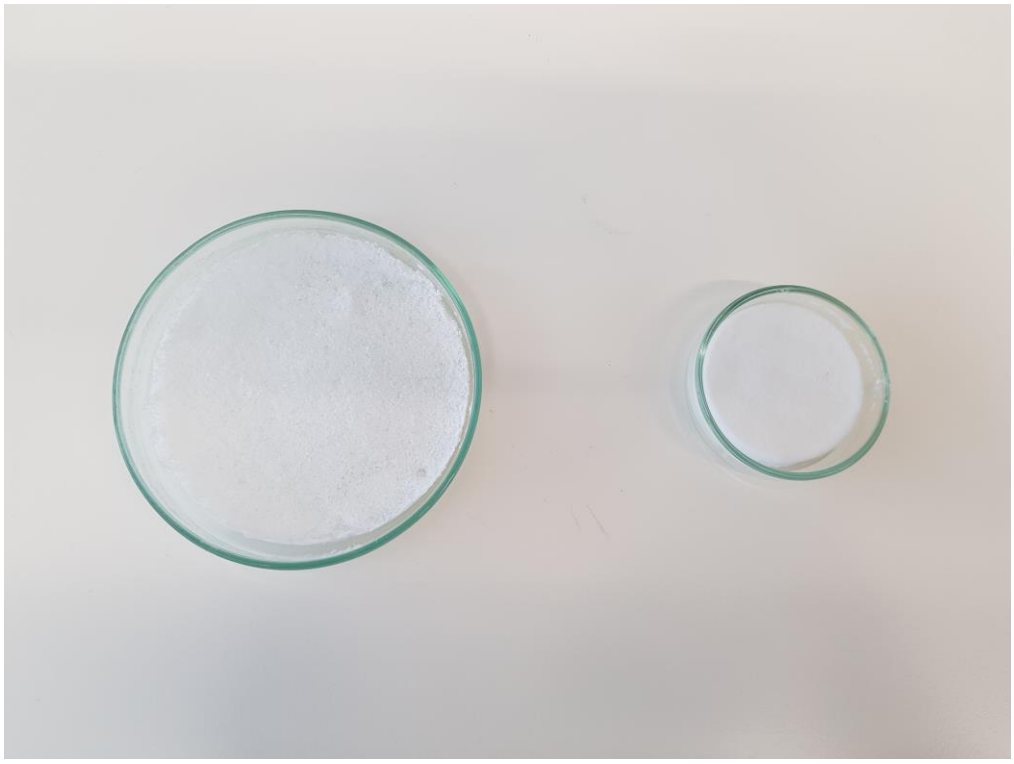

Figure 4 - Collagen-nanoHA scaffolds with 10 and 5 cm of diameter.

3.3 Characterization of the cryogels

3.3.1 Swelling capacity test

The swelling capacity test was done at room temperature to evaluate the ability of the scaffolds to capture and retain a solution. Samples with cubic shape were emerged both in water and aqueous phosphate-buffered saline (PBS). The study was done during 1 hour and the samples were weighed at the beginning of it and after each time-point.

The equilibrium of the absorption – swelling equilibrium (Cw) - was calculated using the formula

$$Cw = \frac{Ws - Wd}{Wd} \quad (1)$$

where Ws corresponds to the weight of the swollen sample after the immersion and Wd to the dry weight (before the immersion in water or PBS). Three samples of each type of scaffold were used and an average was calculated and used to obtain a variation.

3.3.2 Dynamic mechanical analysis

The dynamic mechanical analysis (DMA) assay was done in order to evaluate the mechanical properties of the samples under compression and was conducted in a Tritec2000 dynamic mechanical analyser (Triton Technology, UK).

Samples of parallelepiped form with 5 mm thickness and around 10 mm length were cut and emerged in 10 mL of water for 10 min. The scaffolds were subjected to cycles of compression with frequencies varying between 0.100 Hz and 15 Hz at room temperature.

Three samples of each batch of scaffolds were analysed and an average

was calculated and used to obtain a graphic.

3.3.3 Scanning electron microscopy analysis

Scanning electron microscopy (SEM, FEI Quanta 400FEG) was used to analyse the morphology of the samples as well as the size of up to 20 pores from each scaffold.

The samples were first attached with Araldite™ to an aluminium sample holder and then sputter-coated with palladium-gold (Bal-Tec: SCD 050) to become electrically conductive and be analysed.

3.3.4 Fourier transform infrared spectroscopy

The cryogels were analysed using a Fourier transform infrared (FT-IR) spectrophotometer (Perkin Elmer) in order to study their chemical composition.

The analysis was done in the mode ATR, by compressing the samples until a clear spectrum was shown in the screen and the transmittance peaks were then registered.

Every sample was analysed with a resolution of 4 cm^{-1} and an OPD of 0.2 and 100 scans were performed to obtain each graphic.

3.4 *In vitro* biological studies

3.4.1 Cell culture

L929 and MG63 (ATCC) cells were maintained in Dulbecco's modified eagle medium (DMEM, Gibco) supplemented with 10% (v/v) fetal bovine serum (FBS) (Gibco), 1% (v/v) fungizone and 1% (v/v) penicillin-streptomycin (Gibco).

Cells were kept in a cell culture incubator (Binder, Tuttlingen, Germany) at 37°C and 5% carbon dioxide (CO_2), in a humidified atmosphere. After cell confluence of 90% on a 75 cm^2 T-flask (Nunc), which occurred every 3-4 days, cells were detached using trypsin (0.5%, Gibco) as dissociation reagent. Afterwards, cells were counted using a Neubauer chamber, centrifuged (Eppendorf) at 1200 rpm during 5 minutes and then seeded in new T-flasks.

3.4.2 MTT assay

The MTT (3-(4,5-dimethyl-2-thiazolyl)-2,5-diphenyltetrazolium bromide) assay was used to study the indirect cytotoxicity (ISO 10993-5) of the samples with L929 and MG63 cells.

Parallelepiped samples were incubated overnight in filtered 70% ethanol at 4°C. The samples were then washed twice with 5 mL PBS and washed in 5 mL complete medium (30 min). After that, materials (1 g) were incubated for 24 h into 10 mL of fresh complete medium at 37°C and 5% CO_2.

Cells suspension (100 µL) was cultured in 96-well plates in a concentration of 10^5 cells/well. After 24 hours, the medium was removed and 100 µL of the samples extract was added to the wells in different dilutions (25%, 50% and 100%) and incubated for 1 and 3 days. After the removal of the medium, 100 µL of a MTT solution (0.5 mg/mL, Sigma-Aldrich) was added to each well and the plates were incubated for 4 hours at 37°C protected from light. After the incubation time, the medium was removed and 100 µL DMSO (dimethyl sulfoxide, Merck) was added in every well. The optical density, which is directly correlated with the cells viability percentage, was measured on a microplate reader (Synergy Mx, BioTeK) at the wavelength of 550 nm. The cells viability was calculated by assuming 100% viability of cells from the control group (only fresh complete medium). The blank was composed by only DMSO. Every material was evaluated in triplicate.

3.4.3 Resazurin assay

The resazurin (Alamar blue dye) assay was performed to study the direct cytotoxicity of the samples when in contact with L929 and MG63 cells, through its metabolic activity.

Samples were sterilized as described before and incubated with complete DMEM for 30 minutes at room temperature in 24-well plates (no tissue culture). The medium was removed and 20 µL of cells ($3x10^5$) were added to each sample. The plates were incubated for 2 hours at 37°C and the samples were then covered with complete cell culture medium. The samples were incubated for 1, 7, 14 and 21 days and the medium was changed every three days. After removal of the medium, 1 mL of a solution of 10% resazurin (0.1 mg/mL, Sigma-Aldrich) was added protected from the light and the plates were incubated for 3 hours at 37°C. A solution of 100 µL of each well were transferred to a black 96-well plate (triplicates) and the fluorescent intensity was measured in a fluorometer (Synergy Mx, BioTek) at 530 nm for excitation and at 590 nm for emission. After that, samples were washed twice with PBS and re-incubated with fresh complete cell culture medium.

The seeding of L929 and MG63 cells in Tissue Culture Polystyrene (TCPS) with supplemented DMEM was also performed to analyse cells metabolic activity in the absence of the collagen-nanoHA scaffolds. The blank was composed of only resazurin solution. There were three samples of each materials batch.

3.4.4 Alkaline phosphatase (ALP) activity

After the resazurin assay, samples with MG63 cells from days 14 and 21 were washed twice with PBS, put into an eppendorf with 0.5 mL of milli-Q water and incubated for 1 hour at 37°C. After that, samples were stored at -20°C.

Samples were unfrozen to complete cell lysis, cut in small pieces, homogenized in the vortex for 1 minute and centrifuged (Centrifuge 2-16PK, Sigma) at 2000 rpm for 5 minutes. The supernatant (20 µL) was then transferred

to a 96-well flat-bottom plate (triplicates) and 200 µL of ALP substrate was added according to protocol published before (C. et al., 2013). The blank was prepared using 220 µL of only ALP substrate solution. The ALP activity was measured through the substrate (p-nitrophenol phosphate) hydrolysis. After 1 hour of incubation at 37°C, 10 µL of NaOH (0.02 M) was added to each well to stop the reaction and produce a yellowish colour.

In the same plate, 230 µL of increasing p-Nitrophenol Standard Solutions (P5-P1) for calibration curve were measured in triplicates. The blank (0 nmol) was prepared with 230 µL of NaOH (0.02 M). The calibration curve was produced by plotting the absorbance versus nmol of p-Nitrophenol.

The absorbance was measured in a microplate reader (Synergy Mx, BioTeK) at the wavelength of 405 nm and p-nitrophenol was quantified.

In order to correlate the amount of ALP to the total quantity of protein present in the samples, total protein content was measured using the Lowry's method, according to the manufacturer's recommendations (DC™ protein assay, Bio-Rad).

Briefly, to quantify the total amount of protein, a BSA (bovine serum albumin) standard calibration curve was performed. For that, 4 dilutions of a protein standard were prepared from 1 mg/mL to 0.001 mg/mL as well as a blank of milli-Q water (0 mg/mL). 20 µL of both standard solutions and samples was pipetted to a 96-well flat-bottom plate and 25 µL of reagent A was added to each well. Then, 200 µL of reagent B was also added to each well and the plate was incubated at room temperature for 15 minutes.

The absorbance was measured in a microplate reader (Synergy Mx, BioTeK) at the wavelength of 750 nm.

A calibration curve was produced by plotting the absorbance versus the BSA concentration (mg/mL).

Finally, the amount of ALP was calculated using the equations of both the calibration curves referred before and was expressed in nmol per minutes per mg.

3.4.5 DNA quantification assay

Samples were processed as described in the previous assay and the supernatant was used in order to quantify the amount of DNA present in the samples, according to the manufacturer's recommendations (Quant-iT™ Picogreen® DNA assay, Invitrogen, UK)

Briefly, suspension of each sample (10 µL) was pipetted to a black 96-weel flat-bottom plate (triplicates), as well as a blank composed of milli-Q water, and 90 µL TE buffer (1x) was added in triplicate.

High range standard solutions (1 ng/mL to 1 µg/mL) were prepared from a cDNA stock solution (2 µg/mL).

Each standard solution (100 µL) was pipetted in triplicates to the same plate of the samples. Afterwards, 100 µL of PicoGreen reagent was added to every well (samples and standards) and the plate was incubated for 5 minutes, protecting it from the light.

The fluorescent intensity was measured in a fluorimeter (Synergy Mx, BioTek) with an excitation wavelength of 480 nm (±17) and an emission wavelength of 520 nm (±17).

A calibration curve was produced by plotting the fluorescence of the standard solutions versus the DNA concentration (ng/mL) and the amount of DNA was then calculated in ng/mL. Samples from day 21 were evaluated in duplicate.

3.4.6 Confocal laser scanning microscopy

Confocal laser scanning microscopy (CLSM, Leica SP2 AOBS SE camera) was used to study the morphology of MG63 cells after 21 days of being incubated with samples before and after gamma irradiation.

After the resazurin assay samples were washed twice with PBS and incubated in formaldehyde 4% (Sigma-Aldrich) for 30 minutes at room temperature. The samples were then washed twice with PBS and stored at 4°C.

After the removal of the PBS, the materials were incubated with Triton X100 solution (0.1%, Sigma-Aldrich) for 30 minutes at room temperature and washed twice with PBS. Samples were then incubated with a solution of BSA in PBS for 30 minutes and washed twice with PBS. The cells cytoplasm (phalloidin) was stained with Alexa fluor conjugated phalloidin 594 (1:400, Invitrogen) diluted in BSA solution (1%) for 1 hour at room temperature and protected from light. After that, the samples were washed twice with PBS and the nuclei were stained with DAPI (4'-6-diamidine-2-phenylindole, 1 µg/mL, Sigma-Aldrich) diluted in PBS for 5 minutes. The samples were washed twice in PBS and evaluated by Confocal Laser Scanning Microscopy.

The images were captured using excitation lasers of 405 nm and 594 nm.

After the analysis of cryogels from day 21, samples from day 14 were not imaged since they did not show a considerable amount of cells.

3.4.7 Statistical analysis

Data from *in vitro* assays with cell cultures was presented as mean ± standard deviation, and was analyzed using two-way ANOVA test. Differences between samples were considered statistically significant when $p < 0.05$.

Chapter 4

Results and Discussion

4.1 Characterization of the cryogels

4.1.1 Swelling capacity test

The swelling capacity test was performed to evaluate the ability of the scaffolds to capture and retain solutions (distilled water and PBS) for 60 min.

In Table 2 we can observe the behaviour of the collagen/nanoHA scaffolds A-D (before gamma irradiation) immersed in distilled water and PBS after 2, 15 and 60 minutes.

For all the samples, the uptake of water showed an increase in the first 2 minutes. The Cw value didn't show major differences until it reached 15 minutes, time-point previously indicated in the bibliography as being the equilibrium (C. et al., 2013). The values were similar until the last time-point (60 min).

Table 2 - Swelling kinetics of the scaffolds before irradiation (A-D) in distilled water and PBS.

	Swelling ratio (Cw)					
	H_2O			**PBS**		
Sample	**2 min**	**15 min**	**60 min**	**2 min**	**15 min**	**60 min**
A (Ø10cm)	19.23 ± 0.72	18.82 ± 0.85	19.46 ± 0.41	20.69 ± 0.73	19.87 ± 1.29	21.69 ± 1.20
A (Ø 5cm)	20.74 ± 1.79	21.61 ± 1.90	19.26 ± 2.86	24.99 ± 2.17	23.82 ± 2.77	24.17 ± 1.73
B (Ø10cm)	26.24 ± 1.30	25.30 ± 1.33	26.57 ± 1.70	23.90 ± 1.40	25.56 ± 2.07	23.71 ± 0.53
B (Ø 5cm)	25.07 ± 1.29	24.60 ± 0.88	26.55 ± 0.69	28.09 ± 3.67	25.64 ± 0.90	25.55 ± 1.90
C (Ø10cm)	25.37 ± 1.60	23.53 ± 2.15	23.74 ± 1.58	24.73 ± 0.77	24.93 ± 1.40	25.51 ± 0.71
C (Ø 5cm)	27.01 ± 0.12	26.85 ± 1.10	27.73 ± 1.27	28.69 ± 0.99	27.82 ± 1.67	28.14 ± 1.94
D (Ø10cm)	15.07 ± 0.15	15.03 ± 0.34	15.26 ± 0.32	15.17 ± 0.40	16.28 ± 0.57	16.44 ± 1.11
D (Ø 5cm)	17.51 ± 0.74	16.48 ± 0.58	16.68 ± 0.52	17.30 ± 0.87	16.74 ± 1.49	14.38 ± 1.66

Since the values of Cw were maintained from minute 2 until 60 min, it is possible to conclude that the equilibrium was reached at 2 minutes, as it happened in Jain et al. studies (Jain, Srivastava, & Kumar, 2008). It is possible to see that the samples that showed lower values of the swelling coefficient were the ones from batch D, specially the samples with Ø 10 cm, which had the lowest value when compared to all tested samples. In general, the smaller samples (Ø 5 cm) had higher water uptake when compared to the larger materials (Ø 10 cm).

Regarding the PBS uptake, the results of the absorption coefficient also showed a difference between the scaffolds from different batches, having batch D with Ø 5 cm the lowest value of Cw. The values for the Cw were very similar to the same materials evaluated in the presence of water and the smaller samples were also the materials with higher Cw values.

Table 3 - Swelling kinetics of the scaffolds after irradiation (A'-D') in distilled water and PBS.

	Swelling ratio (Cw)					
	H_2O			**PBS**		
Sample	**2 min**	**15 min**	**60 min**	**2 min**	**15 min**	**60 min**
A' (Ø10cm)	21.25 ± 0.35	22.20 ± 2.19	22.21 ± 1.52	22.42 ± 1,58	21.38 ± 0.62	20.97 ± 0.19
A' (Ø5cm)	24.31 ± 1.10	25.05 ± 0.60	23.65 ± 1.12	21.67 ± 3.42	22.69 ± 1.37	22.75 ± 0.98
B' (Ø10cm)	23.15 ± 0.90	24.72 ± 0.63	24.47 ± 1.33	23.24 ± 0.95	21.94 ± 0.31	23.08 ± 0.84
B' (Ø5cm)	24.01 ± 1.26	24.36 ± 0.87	23.76 ± 2.25	22.62± 2.59	23.39 ± 1.45	24.16 ± 0.89
C' (Ø10cm)	23.29 ± 1.48	23.78 ± 0.83	24.40 ± 0.55	24.24 ± 1.92	27.00 ± 2.12	24.13 ± 1.87
C' (Ø5cm)	24.24 ± 1.17	23.91 ± 1.21	25.34 ± 0.78	25.67 ± 0.52	26.33 ± 1.28	24.79 ± 0.72
D' (Ø10cm)	15.54 ± 2.55	14.21 ± 4.85	14.32 ± 5.07	14.67 ± 0.12	13.82 ± 0.08	11.97 ± 1.79
D' (Ø5cm)	13.90 ± 0.93	14.84 ± 0.29	14.68 ± 1.39	16.83 ± 2.16	13.88 ± 1.51	15.57 ± 1.13

The behaviour of the scaffolds A'-D' (gamma irradiated) after 2, 15 and

60 minutes is represented in Table 3.

As observed in table 2, samples showed similar values of the swelling coefficient for the water evaluation from minute 2 until the end of the study (60 min). The samples D' (Ø 10 cm) showed the lowest values of Cw, in most cases. In the other batches (A'-C'), the larger membranes (Ø 10 cm) were also the ones that presented lower Cw values.

The results of the PBS uptake were similar to the evaluation with water and batch D with Ø 10 cm also showed the lowest value of Cw. Therefore, the smaller membranes performed higher water uptake. The differences between the Ø 10 cm and Ø 5 cm membranes might be related to their porosity and to the fact that these last ones are the first to be released into the molds during the production process of the cryogels, and, in case of low homogenization of the solution, they will have a composition different from the Ø 10 cm membranes.

Comparing the results of the samples before (A-D) and after gamma irradiation (A'-D'), it is possible to observe a higher water uptake before irradiation. The PBS uptake by the irradiated scaffolds was also lower, being the non-irradiated samples the ones with higher values of Cw. Comparing batch D, which presented lower values before and after sterilization, the lower Cw was observed in the material D' with Ø 10 cm (11.97 ± 1.79).

The fastest water uptake, showed after the first 2 minutes of our study, is closely related to a higher interconnectivity of the pores and hydrophilicity of the material, which is the objective of the scaffold for clinical applications, since it allows a higher dissipation of molecules, nutrients, gases or fluids throughout the material (Jain et al., 2008). In comparison, the hydrogels water uptake is a slower process since it is dependent on the water diffusion (Jain et al., 2008). Furthermore, scaffolds that retain a higher amount of water are associated with the presence of larger pores (Hoffman, 2012; Nieto-Suárez, López-Quintela, & Lazzari, 2016). This higher retention of water will result in swelling capacity of the scaffolds, which will expand the materials structure that is available for cell migration and adhesion, because of a closer contact with the surrounding tissue (Wu et al., 2010). However, the higher retention of water can also decrease the mechanical properties of the scaffold, by also decreasing its elastic strength (Sowjanya et al., 2013). Therefore, the objective for the final clinical application is a structure with interconnected pores that will allow an equilibrium between the swelling capacity and the mechanical

properties, without compromising any of them. In this study, these properties correspond to the materials with lower Cw values.

The samples from batch D showed better swelling capacity with both water and PBS, before and after irradiation, closer to the results observed in previous studies that were 18.54 (water) and 17.56 (PBS) after 15 minutes for collagen-nanoHA (30:70% wt) scaffolds. As for collagen-nanoHA (50:50% wt) scaffolds, the values were higher, 28.63 (water) and 30.04 (PBS) (C. et al., 2013).

As mentioned in chapter 3, the collagen used for batch D was from a different source in comparison to the other cryogels (A-C). In this batch, the purchased collagen was already dissolved, so the collagen stability (degradation) could had been compromised since the solution pH was very acidic (pH<2). As observed, batch D results showed the lowest values of Cw. These samples also had higher porosity (Fig. 8), which could compromise the materials handling without damaging the porous structure. All the other batches (A-C) had similar results, but batch A with Ø 10 cm (19.23± 0.72) presented lower values of Cw. The differences between batches A-C might be related to difficulties in performing an adequate homogenization of the collagen-nanoHA in the reactor during the materials' production. Thus, samples with a higher concentration of nanoHA are connected to a lower swelling ratio. This could be explained by the lower hydrophilicity of hydroxyapatite and by the fact that, when combined with collagen, the calcium and phosphate of hydroxyapatite will bind to the hydrophilic groups of collagen (COOH and NH_2), resulting in a decrease in the overall sample hydrophilicity (A. Sionkowska & Kozłowska, 2013).

Although, the results were similar to previous studies (C. et al., 2013), the protocol can be revised and optimized in order to obtain scaffolds with lower values of Cw and higher mechanical properties.

4.1.2 Dynamic mechanical analysis

The dynamic mechanical analysis (DMA) assay was performed in order to evaluate the mechanical properties of the cryogels under dynamic compressive

stress state.

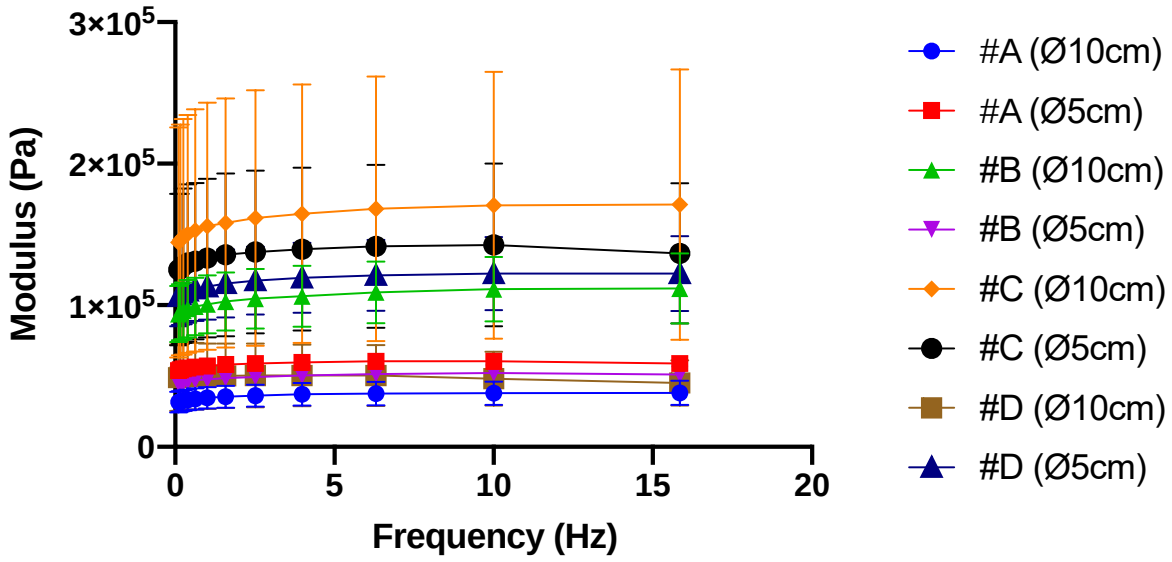

Figure 5 - Storage modulus (E') of samples A-D under dynamic compression solicitation versus increasing frequency, ranging from 0.1 to 15 Hz.

Figure 5 shows the variation of the storage modulus (E') for samples A-D, which refers to the elastic component of a material (Torres, Nazhat, Sheikh Md Fadzullah, Maquet, & Boccaccini, 2007), with respect to the frequency. The higher the storage modulus, the higher the stiffness of the material.

All of the samples showed a rise of E' as the frequency increased, until 10.000 Hz. It is also possible to observe that the scaffolds from batch C with Ø 10 cm had higher modulus values when compared with all the other evaluated samples (A, B and D).

Figure 6 represents the loss factor (Tan Delta), which is the ratio between the loss modulus (E'') and the storage modulus (E') and is related to the viscoelastic behaviour of the material (Torres et al., 2007), with respect to the frequency.

The results obtained were similar for the majority of the samples until 10.000 Hz, although the scaffolds from batch A with Ø 10 cm showed lower loss factor values.

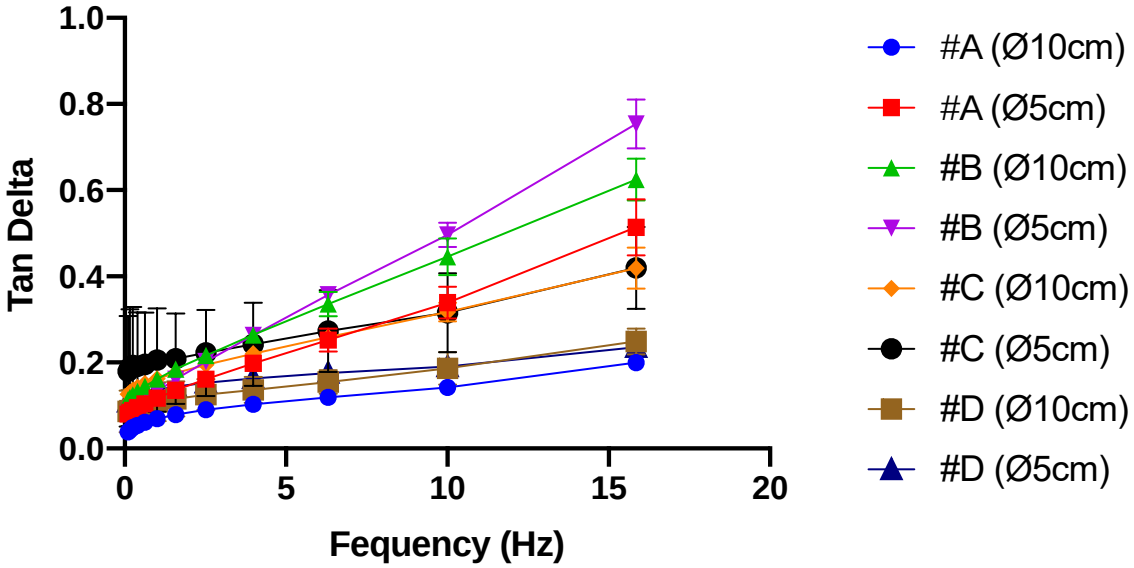

Figure 6 – Loss factor (Tan delta) of samples A-D under dynamic compression solicitation versus increasing frequency, ranging from 0.1 to 15 Hz.

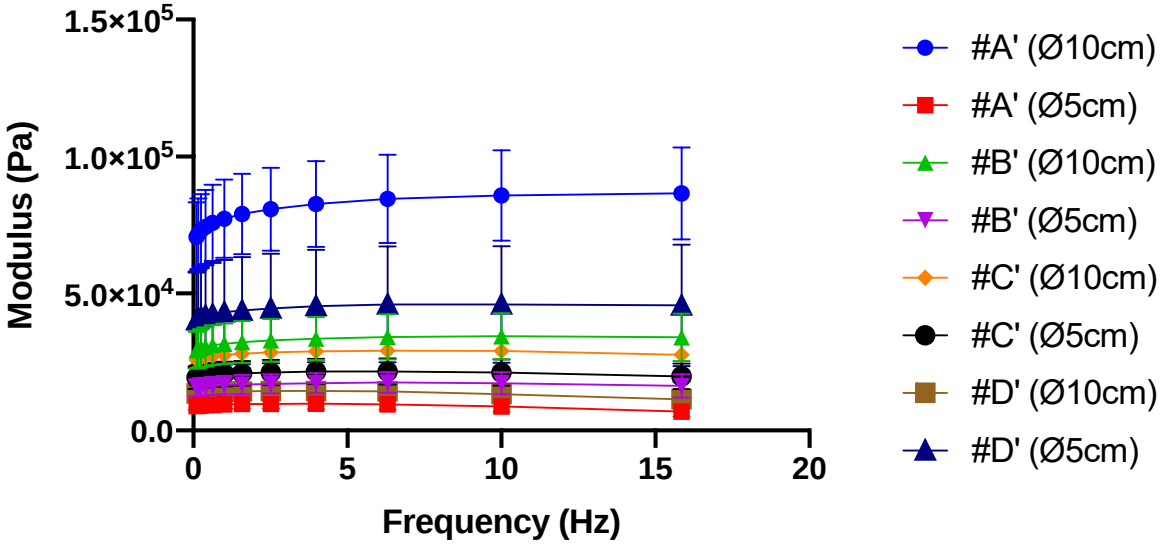

Figure 7 – Storage modulus (E') of samples A'-D' under dynamic compression solicitation versus increasing frequency, ranging from 0.1 to 15 Hz.

In Figure 7 we can observe the results of E' with respect to the frequency for materials A'-D'.

Moreover, all the evaluated samples showed increasing values of the storage modulus as the frequency increases until 10.000 Hz, but in this analysis, samples from batch A with Ø 10 cm showed higher E' values.

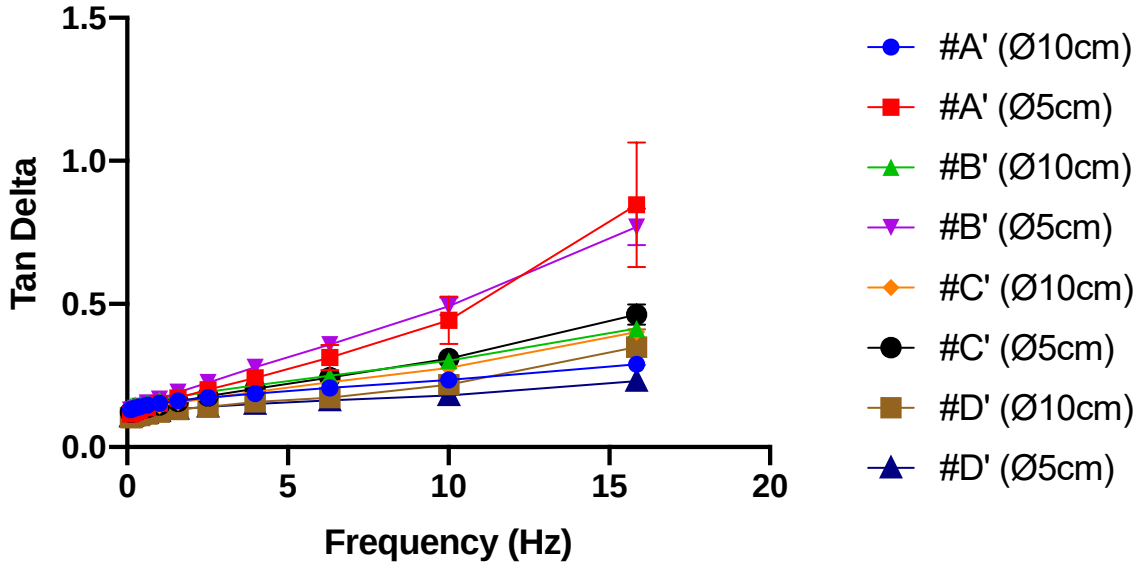

Figure 8 - Loss factor (Tan delta) of samples A-D under dynamic compression solicitation versus increasing frequency, ranging from 0.1 to 15 Hz.

Finally, Tan delta results with respect to the frequency for the materials after gamma irradiation are represented in Figure 8.

The loss factor values were similar between most of the evaluated samples (with the exception of materials A' and B', both with Ø 5 cm) until 10.000 Hz, but batch D' with Ø 5 cm showed lower Tan Delta values, in contrary to previous results from the same batch that was not irradiated (D).

Comparing the results from the materials before and after irradiation, it is possible to observe that samples A-D reached higher values of E' and lower values of Tan delta in higher frequencies. These discrepancies between all the materials batches may be a result of a heterogeneity of nanoHA solution dispersion into the collagen solution during the homogenization process into the reactor. Higher concentrations of nanohydroxyapatite will lead to a

decrease in the loss factor and an enhancement of the storage modulus (C. et al., 2013; Laranjo et al., 2016), showing higher stiffness of the material. Nevertheless, within the same batch, the results from both evaluated parameters (E' and Tan delta) were also different before and after gamma irradiation, which could have been affected by some alteration in the collagen chains induced by energy generated by the radiation. According to previous works, gamma radiation induces an increase of collagen fibrils diameter, leading to their aggregation and resulting in a striated surface, but maintaining the cross-link. This will lead to a decrease in the solubility of the protein and its fragmentation, which can explain the differences observed in the mechanical properties of samples A-D and A'-D' (Bowes & Moss, 1962; Leontiou, Matthopoulos, Tzaphlidou, & Glaros, 1993; B. Liu, Harrell, Davis, Dresden, & Spira, 1989).

The increase of the E' is related to material's higher stiffness and mechanical resistance. Sandra C. Rodrigues et. al. (2013) had observed a faster increase in the E' as the frequency increases, followed by a stabilization of the storage modulus value. However, their study showed higher E' results when compared with the similar materials evaluated in this work showed in Figures 5 and 7 (C. et al., 2013). Studies performed by Salgado et. al. (2016) also showed an increase of the storage modulus with the enhancement of the frequency applied to the materials. Nonetheless, as mentioned before, their study showed higher E' results when compared with the results presented in Figures 5 and 7 (Laranjo et al., 2016). Moreover, the studies presented by Sandra C. Rodrigues et. al. (2013) showed an enhancement of Tal Delta as the frequency increased with values varying between 0.2 and 0.8 (C. et al., 2013). The enhancement of the loss factor shows a more viscous and less elastic behaviour of the material, so the ideal materials response would be a lower value of the loss factor. Having this in consideration, it was shown that sample A' with Ø 10 cm presented higher values of E' and lower values of Tan delta. Through the analysis of the results, it was also possible to observe that the larger scaffolds (Ø 10 cm) presented higher values of E' and lower values of Tan delta and, therefore, the material could be used to the proposed clinical application.

4.1.3 Scanning electron microscopy analysis

Scanning electron microscopy (SEM) was used to analyse the morphology of the scaffolds as well as the size of up to 20 pores from each scaffold.

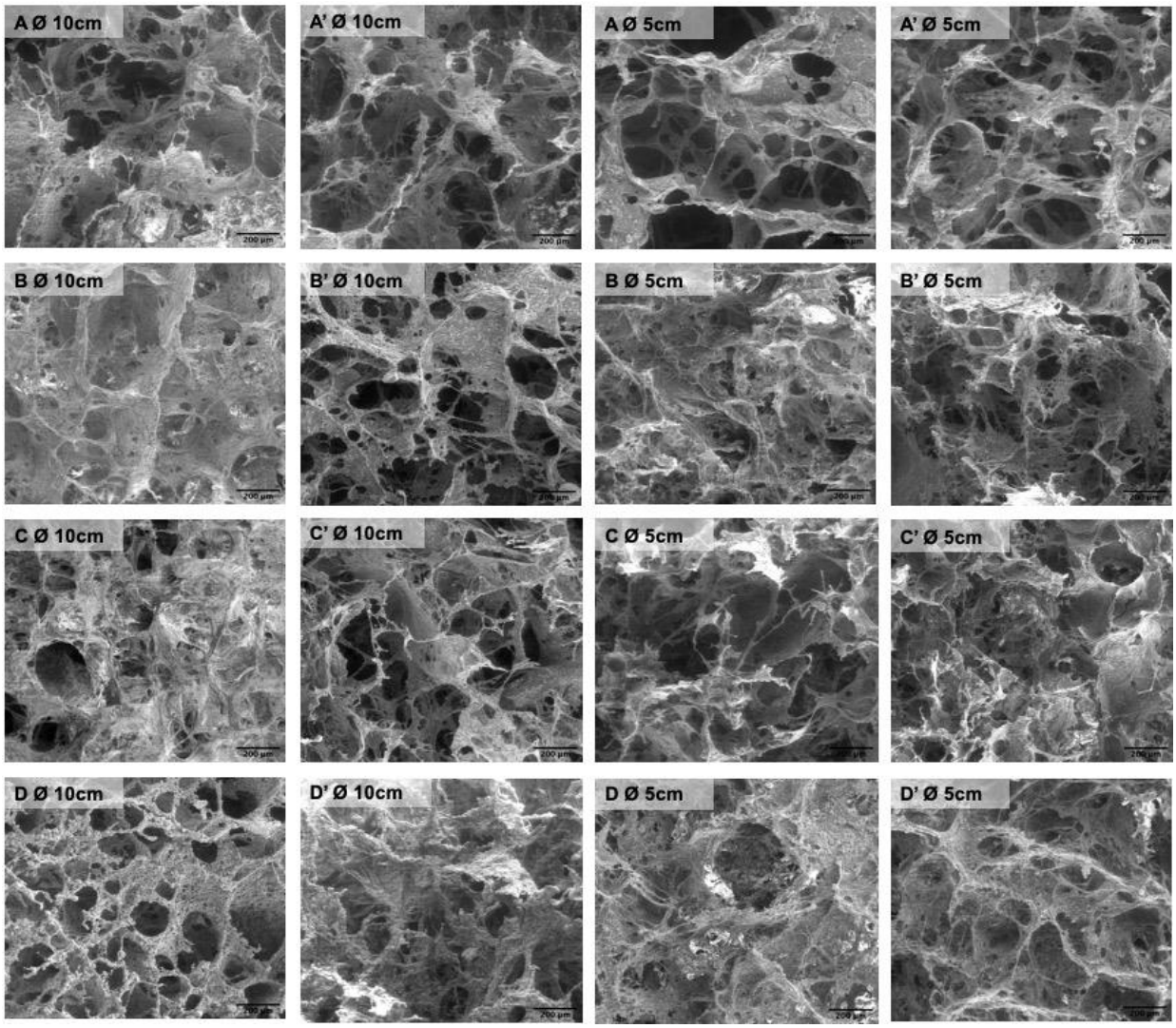

Figure 9 - SEM images of scaffolds A-D and A'-D'. Scale bar: 200 µm.

Figure 9 shows the SEM images of the samples surface before and after gamma irradiation.

In Figure 9, it was shown in the microscope images that all the scaffolds presented interconnected pores of different sizes. In corroboration with

previous results showed in this work, the materials from batch D with Ø 10 cm, both irradiated and non-irradiated, presented higher number of pores and, because of that, they were hard to handle, being damaged by manipulation. It was also possible to observe that irradiation did not have an impact on the scaffolds porosity, since no major differences have been observed during the analysis. Between the largest (Ø 10 cm) and smallest (Ø 5 cm) size membranes, there were no significant differences in pores dimensions. In images with higher magnifications (Fig. 10), spherical aggregates of nanoHA could be observed in the scaffolds, probably due to problems in the homogenization step of the ceramic powder during the production of the cryogels. These aggregates are similar to the ones observed in the nanoHA granules studied by Laranjeira et al. (Laranjeira, Fernandes, & Monteiro, 2010).

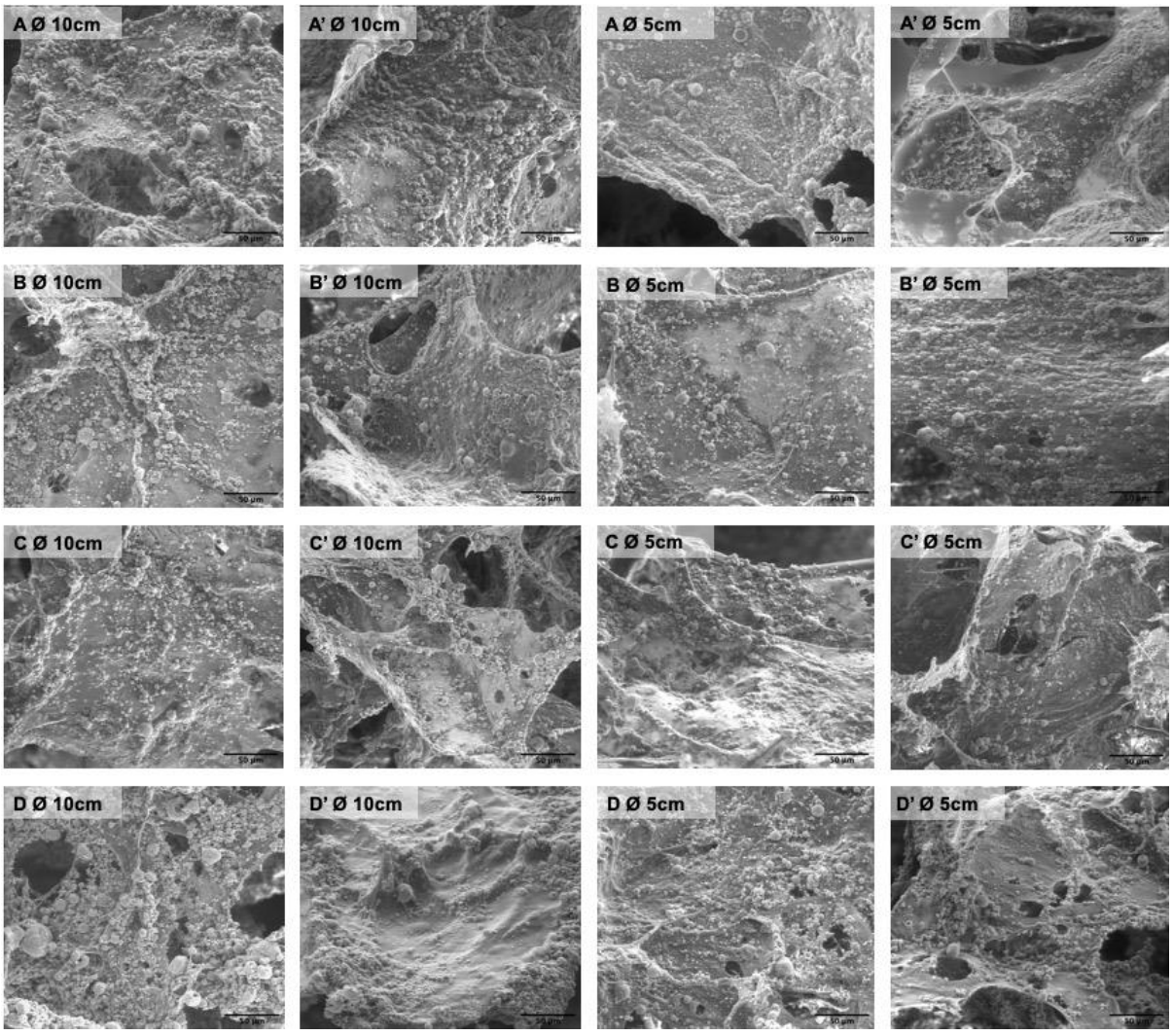

Figure 10 - SEM images of scaffolds A-D and A'-D'. Scale bar: 50 µm.

Table 4 - Average, maximum and minimum pore diameter of samples A-D.

Sample	Average pore diameter (μm)	Maximum pore diameter (μm)	Minimum pore diameter (μm)
A (Ø 10cm)	191.49 ± 107.57	429.20	66.26
A (Ø 5cm)	338.10 ± 196.51	707.10	84.34
B (Ø10cm)	246.79 ± 101.93	451.40	78.10
B (Ø 5cm)	138.34 ± 84.55	283.10	45.00
C (Ø 10cm)	270.81 ± 106.51	511.40	114.10
C (Ø 5cm)	203.27 ± 104.65	420.20	69.16
D (Ø 10cm)	163.36 ± 61.40	306.20	71.96
D (Ø 5cm)	208.86 ± 74.84	403.30	118.80

Table 5 - Average, maximum and minimum pore diameter of samples A'-D'.

Sample	Average pore diameter (μm)	Maximum pore diameter (μm)	Minimum pore diameter (μm)
A' (Ø 10cm)	318.95 ± 259.55	943.30	38.75
A' (Ø 5cm)	237.34 ± 186.71	790.50	61.50
B' (Ø10cm)	160.92 ± 89.68	334.00	62.91
B' (Ø 5cm)	244.08 ± 200.69	814.70	52.87
C' (Ø 10cm)	152.91 ± 65.82	287.90	44.10
C' (Ø 5cm)	173.92 ± 128.36	549.30	64.06
D' (Ø 10cm)	333.36 ± 176.95	620.30	157.60
D' (Ø 5cm)	180.81 ± 129.42	615.70	53.76

To obtain more information regarding the porosity of the scaffolds produced, the size of up to 20 pores from each material were measured and the results are presented in Tables 4 and 5.

As observed in Figure 9, the pores of all samples were very heterogeneous with sizes varying from 38.75 µm to 943.30 µm, which gave the materials' both microporosity and macroporosity. This was an important characteristic, since pores with size larger than 100 µm should be essential for cell seeding and tissue ingrowth whereas pores with diameters higher than 140 µm are important to promote angiogenesis (Fierz et al., 2008; Idaszek, Kijeńska, Łojkowski, & Swieszkowski, 2016; Klenke et al., 2008; Rücker et al., 2008; Singh et al., 2009; Wei et al., 2010). From the results of both tables, it is possible to observe that the non-irradiated scaffolds presented larger pore size. As mentioned before, gamma irradiation does not have an effect on collagen cross-linking, so it should not have an effect on pores sizes (Bowes & Moss, 1962; Leontiou et al., 1993; B. Liu et al., 1989). Thus, the differences might also be explained by the fact that a reduced number of pores were analysed and thus the values might not be in full agreement with the total and actual porosity of the materials. About the comparison between the scaffolds with Ø 10 cm and Ø 5 cm, no correlation could be established, since the irradiated samples showed larger pores and, in contrast, non-irradiated samples showed smaller pores.

In previous studies, scaffolds of collagen/nanoHA 50:50% wt produced by Sandra C. Rodrigues also showed an heteroporous morphology with pores of an average size of 74.39 ± 49.05 µm, being the maximum size 322.09 µm and the minimum 12.16 µm (C. et al., 2013). In comparison to these results, our materials showed higher maximum pore size. Collagen-nanoHA (50:50% wt) scaffolds produced by Sionkowska et al. also showed an heteroporous morphology with pore sizes varying from 50 to 150 µm (A. Sionkowska & Kozłowska, 2013).

4.1.4 Fourier transform infrared spectroscopy

Fourier transform infrared spectroscopy (FT-IR) attenuated total reflectance (ATR) measures absorption and emission of infrared light of a

sample at each wavelength that originate a spectrum. FT-IR was used to characterize the chemical groups present in the cryogels in order to observe their composition.

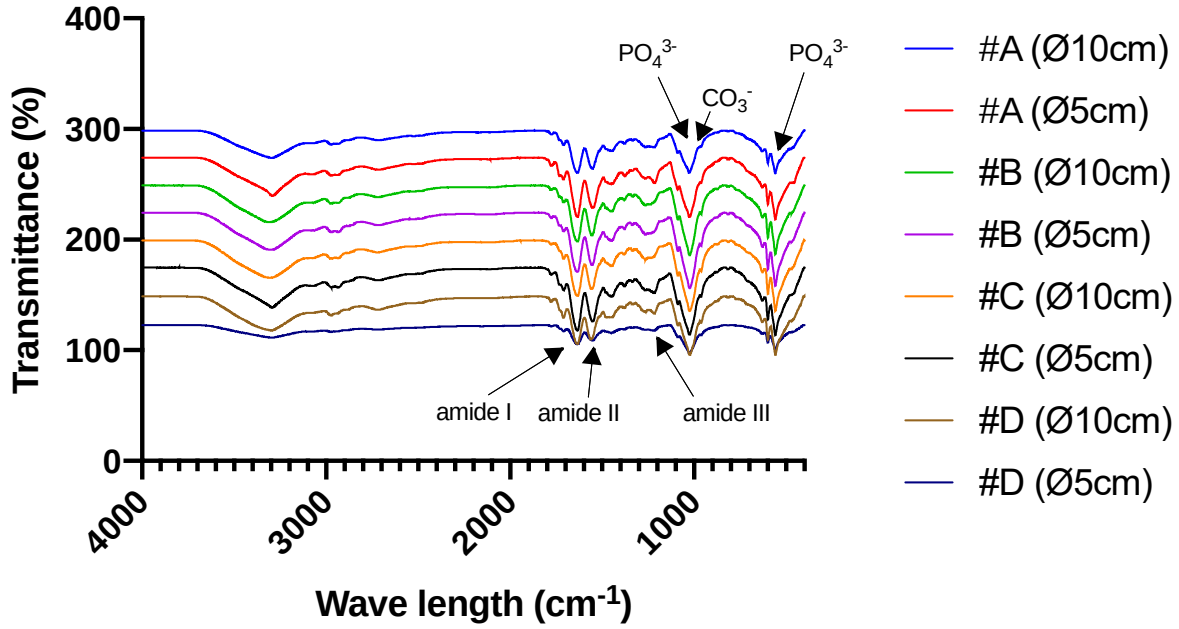

Figure 11 - FT-IR spectra of samples A-D.

In Figure 11 we can see the spectra of FT-IR analysis for samples before gamma irradiation.

The characteristic bands of collagen can be seen at 1648 cm^{-1}, which refer to the amide I (C=O stretching), 1550 cm^{-1}, correspondent to the amide II (N-H deformation), and 1239 cm^{-1}, which is the amide III (N-H deformation) (Chang & Tanaka, 2002).

The peaks of the nanoHA, which result from the vibration of the phosphate groups (PO_4^{3-}), are also represented at 1031 cm^{-1} (V3 and V1 modes vibration of PO_4^{3-}), 962 cm^{-1} (V3 and V1 mode), 602 cm^{-1} (V4 mode) and 564 cm^{-1} (V4 mode). The band of carbonate (CO_3^{-}, v2 vibration) is observed at 875 cm^{-1} (Chang & Tanaka, 2002).

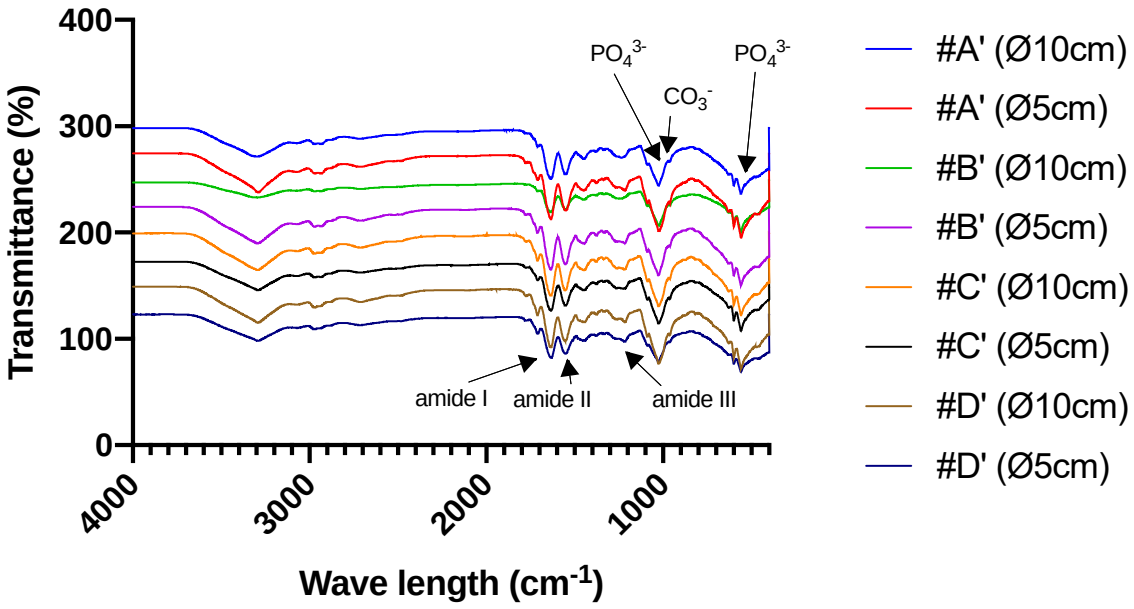

Figure 12 - FT-IR spectra of samples A'-D'.

The FT-IR spectra for irradiated samples (A'-D') is showed in Figure 12.

The characteristic bands of collagen and nanoHA are also present in these spectra.

In the scaffolds A-D and A'-D', like in the materials produced by Sandra Rodrigues, the peak of amide I appears at 1648 cm^{-1} and not at 1658 cm^{-1}, when the collagen is not combined, probably due to the interaction of nanoHA and collagen through carbonyl groups (C. et al., 2013; Lima, Resende, de Almeida Soares, Anselme, & Almeida, 2013).

4.2 *In vitro* biological studies

4.2.1 MTT assay

The MTT assay is a colorimetric assay that is used to assess cell viability. This assay is based on the reduction of 3-(4,5-dimethyl-2-thiazolyl)-2,5-

diphenyltetrazolium bromide (MTT), which is a tetrazolium dye with a yellow colour, to purple formazan by mitochondrial dehydrogenases (Patravale, Dandekar, & Jain, 2012). The higher the cellular viability, the more intense the purple colour measured as optical density.

In our study, the MTT assay was used to determine the indirect cytotoxicity of the samples A-D and A'-D'. Extracts of all samples were in contact with L929 and MG63 cells for 1 day and 3 days of incubation according to ISO 10993-5.

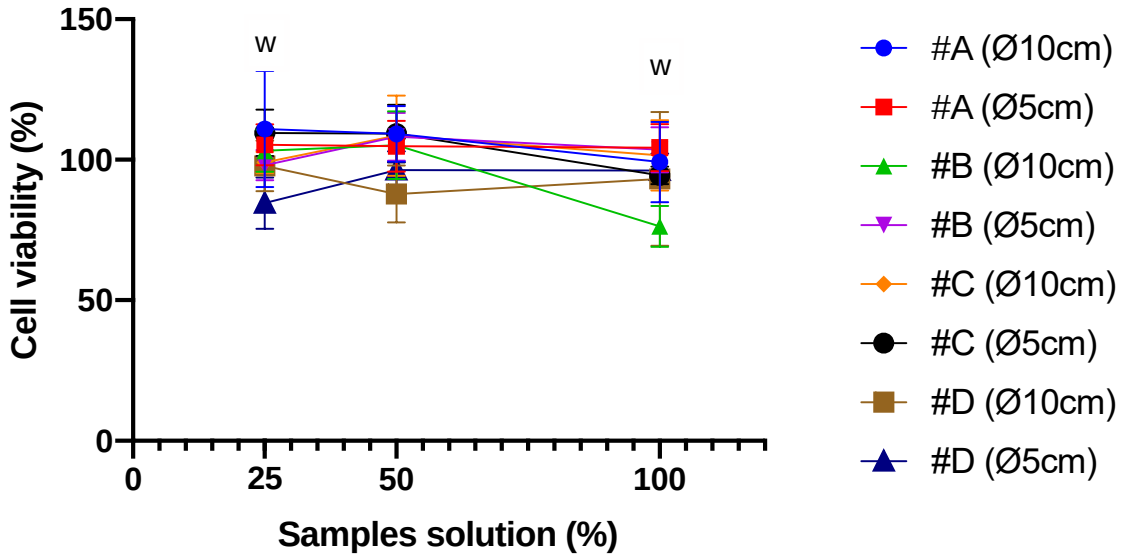

Figure 13 - Cell viability of L929 when in contact with extracts of samples A-D in 3 different concentrations (25%, 50% and 100%) after 1 day of incubation estimated by MTT assay. Control was done in TCPS and considered to have cell viability of 100%. Statistically significant difference at 25% dilution between #D (Ø5cm) and both #A (Ø10cm) and #C (Ø5cm) (w - $p<0.05$). Statistically significant difference at 100% dilution between #B (Ø10cm) and #A (Ø5cm) and #B (Ø5cm) and #C (Ø10cm) (w - $p<0.05$).

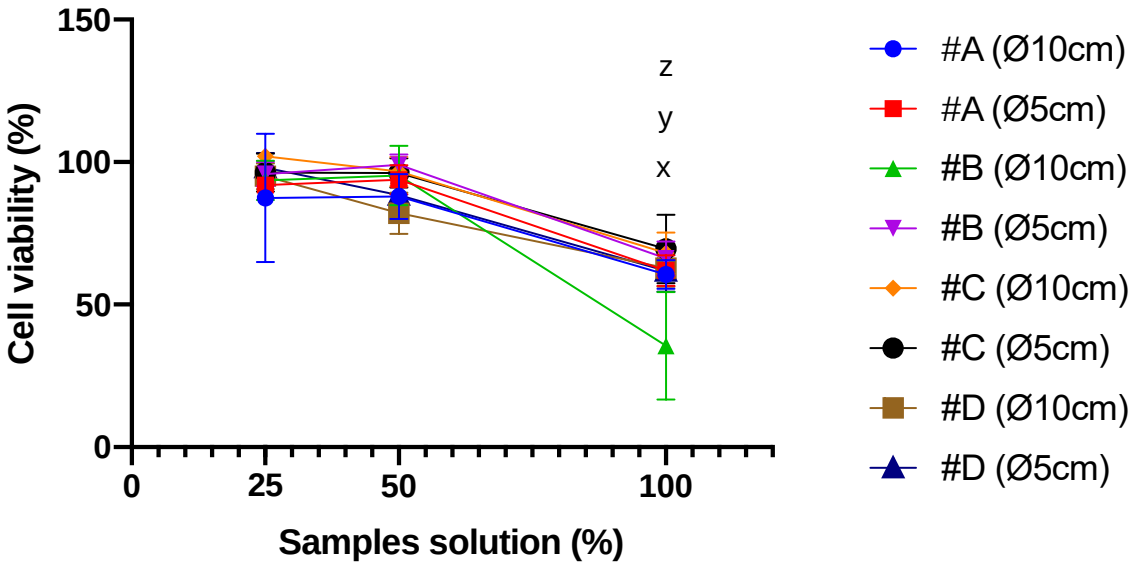

Figure 14 - Cell viability of L929 when in contact with extracts of samples A-D in 3 different concentrations (25%, 50% and 100%) after 3 days of incubation estimated by MTT assay. Control was done in TCPS and considered to have cell viability of 100%. Statistically significant difference between: #A (Ø10cm) and #B (Ø10cm) (x - $p<0.01$); #B (Ø10cm) and both #A (Ø5cm) and #D (Ø10cm and (Ø5cm) (y - $p<0.001$); #B (Ø10cm) and both #B (Ø5cm) and #C (Ø10cm and Ø5cm) (z - $p<0.0001$).

Figures 13 and 14 represent the cellular viability of L929 cells when in contact with extracts of samples A-D in different concentrations (25%, 50% and 100%) after 1 day and 3 days of incubation, respectively.

After 1 day, the higher concentration of material's extract (100%) showed a cell viability close to 100%, except for material B with Ø 10 cm. Dilutions of 25% and 50% of the material's extract showed similar cell viability, which indicated a lack of cytotoxicity of all the samples. The highest cellular viability was observed in sample A with Ø 10 cm of dimension.

On day 3, the highest values for cell viability were observed at the dilutions of 25% and 50% of the material's extract when compared to the non-diluted solutions. At 100% concentration, there was a significant difference between sample B with Ø 10 cm, which showed lower cell viability, and all the other samples. However, materials showed a decrease in cellular viability from day 1 to day 3 that could be an accumulative effect of degradation components of the materials into promoting a soft cytotoxicity that isn't unfeasible for their *in vivo* application.

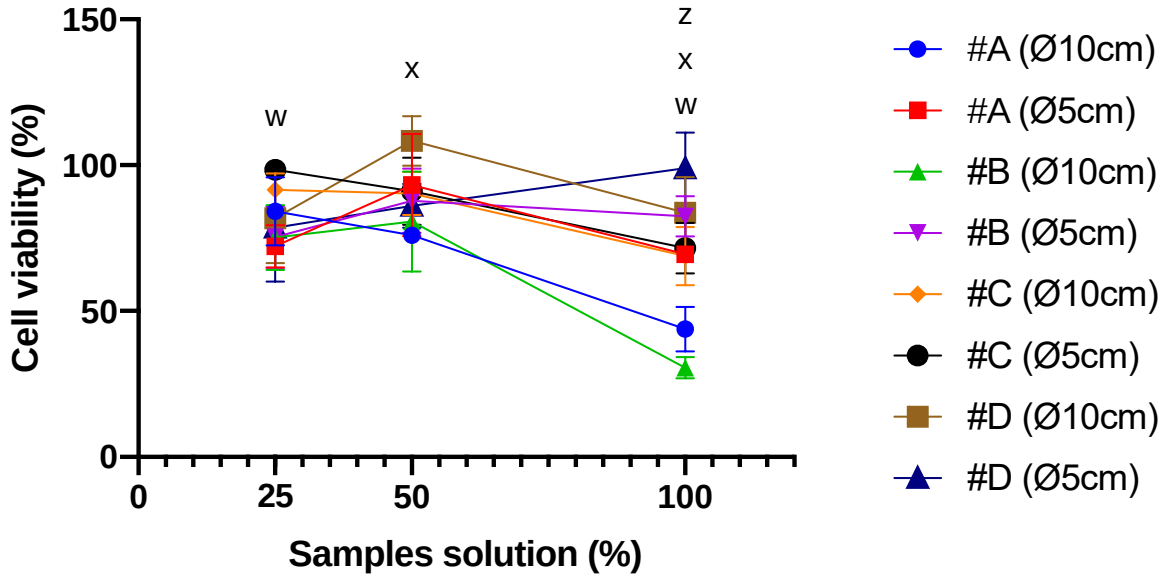

Figure 15 - Cell viability of MG63 when in contact with extracts of samples A-D in 3 different concentrations (25%, 50% and 100%) after 1 day of incubation estimated by MTT assay. Control was done in TCPS and considered to have cell viability of 100%. Statistically significant difference at 25% between #A (Ø5cm) and #C (Ø5cm) (w - $p<0.05$). Statistically significant difference at 50% between #D (Ø10cm) and both #A (Ø10cm) and #B (Ø10cm) (x<0.01). Statistically significant difference at 100% between: #A (Ø10cm) and #A (Ø5cm), and #B (Ø10cm) and #D (Ø10cm) (w - $p<0.05$); #A (Ø5cm) and #D (Ø5cm) (x - $p<0.01$); #B (Ø10cm) and #A (Ø5cm), #B (Ø5cm), #C (Ø5cm) and #D (Ø10cm Ø5cm) (z - $p<0.0001$).

The results of MG63 cells viability when in contact with extracts from samples A-D of the 3 different concentrations (25%, 50% and 100%) throughout 1 and 3 days of incubation can be observed in Figures 15 and 16, respectively.

After 24 hours of incubation, only sample D with Ø 10 cm showed a higher cell viability in the concentration of 100% when compared to the extract dilutions, which shows a cytotoxicity of the samples. This toxicity was slight for all the samples except for samples A with Ø 10 cm and B Ø 10 cm, where it was severe. Furthermore, with the dilution of the extracts, the cytotoxicity effect of the materials reduced and the cell viability increased. This effect leads to the dilution of the degradation products of the materials that could be involved on the cellular cytotoxicity. In all the concentrations, there was a significant

difference between the samples with the same size. At 100% concentration, there was a significant difference between samples A and B, both with Ø 10 cm, and the rest of the materials.

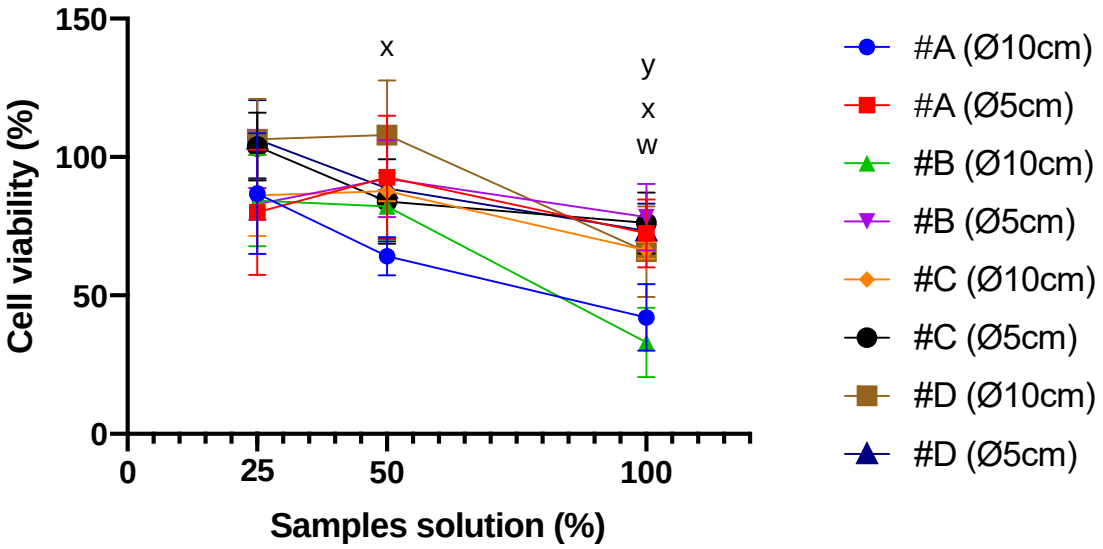

Figure 16 - Cell viability of MG63 when in contact with extracts of samples A-D in 3 different concentrations (25%, 50% and 100%) after 3 days of incubation estimated by MTT assay. Control was done in TCPS and considered to have cell viability of 100%. Statistically significant difference at 50% between #A (Ø10cm) and #D (Ø10cm) (x - $p<0.01$). Statistically significant difference at 100% between: #A (Ø10cm) and #B (Ø5cm), and #B (Ø10cm) and #C (Ø5cm) (w - $p<0.05$); #B (Ø10cm) and #A (Ø5cm), #C (Ø5cm) and #D (Ø5cm) (x - $p<0.01$); #B (Ø10cm) and #B (Ø5cm) (y - $p<0.001$).

On day 3, the values for cellular viability were similar in all the samples compared after 1 day of culture, which shows that some of the degradation products of the materials analysed were not cytotoxic and the cells recovered their viability after 3 days of incubation (batches C and D) and that some samples presented a longer term negative effect on the cellular viability (A and B). This lower cellular viability could be related to a higher degradation rate of the samples with higher release of calcium ions which could be responsible for a decrease in cell viability values. Once again, samples A and B (Ø 10 cm) showed a significant difference when compared to the other materials due to their low cellular viability results.

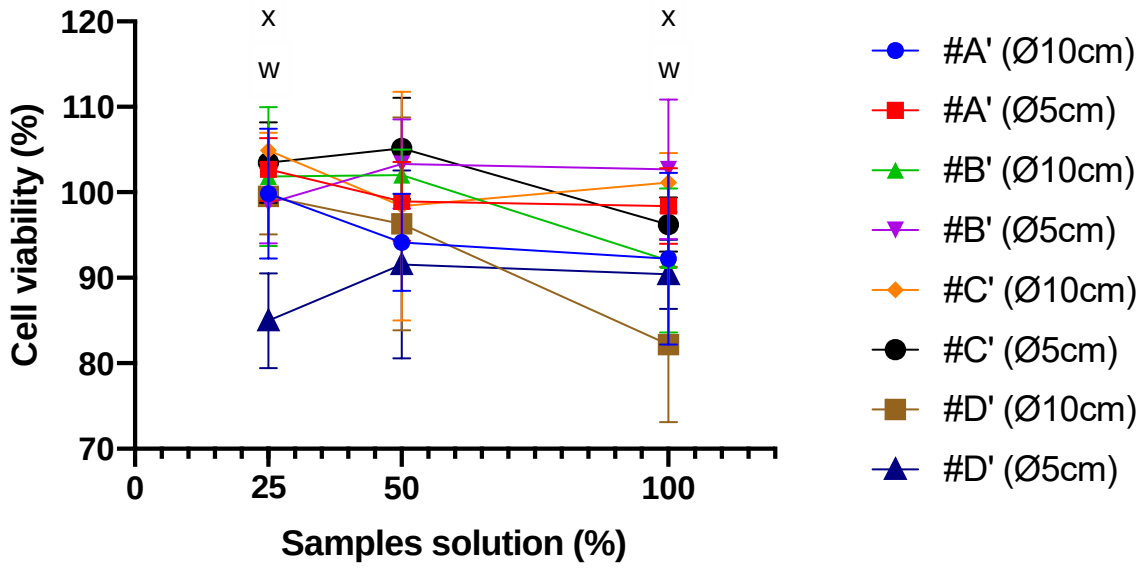

Figure 17 - Cell viability of L929 when in contact with extracts of samples A'-D' in 3 different concentrations (25%, 50% and 100%) after 1 day of incubation estimated by MTT assay. Control was done in TCPS and considered to have cell viability of 100%. Statistically significant difference at 25% between: #D' (Ø5cm) and both #B' (Ø10cm) and #A' (Ø5cm) (w - $p<0.05$); #D' (Ø5cm) and #C' (Ø10cm and Ø5cm) (x - $p<0.01$). Statistically significant difference at 100% between: #D' (Ø10cm) and #A' (Ø5cm) (w - $p<0.05$); #D' (Ø10cm) and both #B' (Ø5cm) and #C' (Ø10cm) (x - $p<0.01$).

Figure 17 shows the cellular viability of L929 cells in contact with A'-D' extracts with dilutions of 25%, 50% and 100% after 1 day of incubation. Figure 18 represents the cell viability after an incubation of 3 days.

In accordance with the previous results showed with fibroblast culture (Fig. 13), after 1 day incubation, similar cell viability results were observed for all extracts dilutions, except for samples D' with Ø 10 cm which should be related to soft toxicity of the sample. At 100% concentration, this scaffold showed a significant decrease in cell viability when compared to all the other samples. Sample D' (Ø 5 cm) showed a significant cell viability decrease compared to the other materials at 25% concentration.

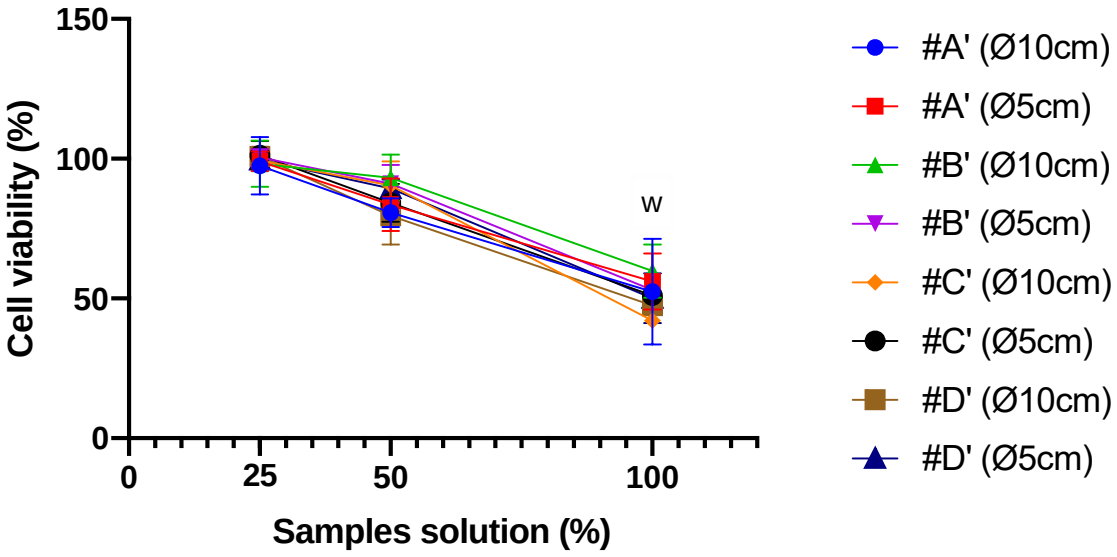

Figure 18 - Cell viability of L929 when in contact with extracts of samples A'-D' in 3 different concentrations (25%, 50% and 100%) after 3 days of incubation estimated by MTT assay. Control was done in TCPS and considered to have cell viability of 100%. Statistically significant difference at 100% between #B' (Ø10cm) and #C' (Ø10cm) (w - $p<0.01$).

After 3 days of incubation, all the samples extracts with a dilution of 25% showed higher cell viability. For the concentration of 100%, the cell viability decreased with cellular viability near to 50%, which reveals light cytotoxicity at higher concentration of the materials' degradation products.

In all the samples there was a decrease of cellular viability after 3 days of incubation, probably due to the accumulation of the negative effect of the scaffolds' degradation products on the cell culture as described before.

Figures 19 and 20 show the results of the human osteoblast-like cells (MG63) cellular viability after 1 and 3 days of incubation, respectively, with samples extracts of 25%, 50% and 100% concentrations.

On day 1, cell viability was similar throughout all the extracts dilutions, except for sample D' with Ø 10 cm and sample A' with Ø 5 cm. In the concentrations of 25% and 50% these samples showed significantly higher and lower cell viability, respectively.

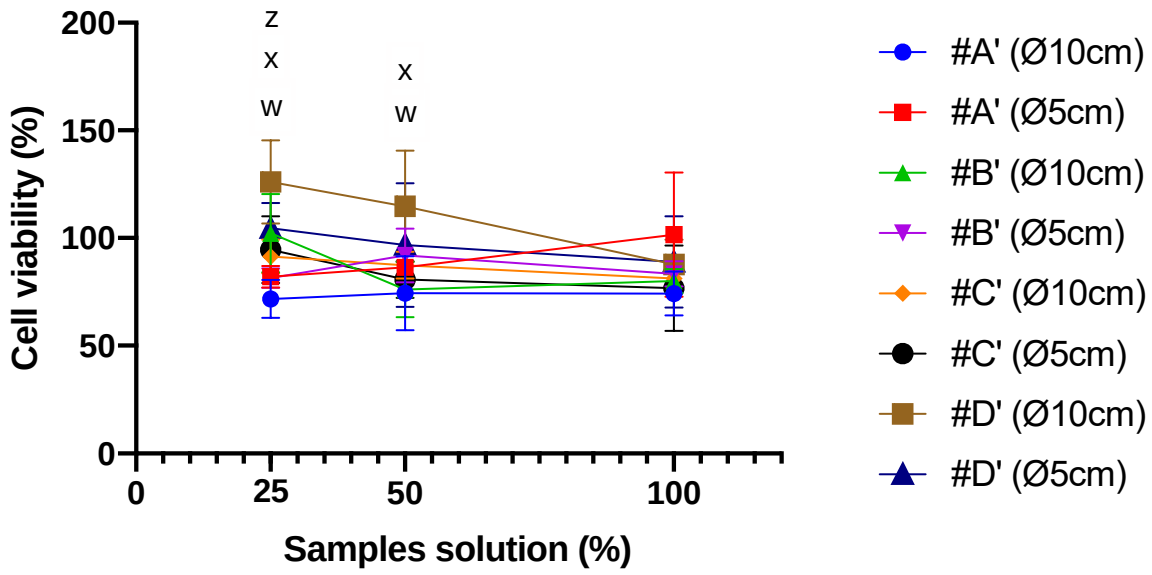

Figure 19 - Cell viability of MG63 when in contact with extracts of samples A'-D' in 3 different concentrations (25%, 50% and 100%) after 1 day of incubation. Control was done in TCPS and considered to have cell viability of 100% estimated by MTT assay. Statistically significant difference at 25% between: #C' (Ø10cm) and #D' (Ø10cm) (w - $p<0.05$); #D' (Ø10cm) and both #A' (Ø5cm) and #B' (Ø5cm) (x - $p<0.01$); #A' (Ø10cm) and #D' (Ø10cm) (z - $p<0.0001$). Statistically significant difference at 50% between: #D' (Ø10cm) and both #B' (Ø10cm) and #C' (Ø5cm) (w - $p<0.05$); #A' (Ø10cm) and #D' (Ø10cm) (x - $p<0.01$).

After 3 days, the opposite response was observed when compared to day 1, as all the materials extract without dilution (100%) showed a decrease on cell viability. However, a similar effect was observed with the fibroblast culture (L929, Fig. 16 and 17). The results of sample D with Ø 10 cm were significantly higher when compared to the other samples at the concentrations of 25% and 100%.

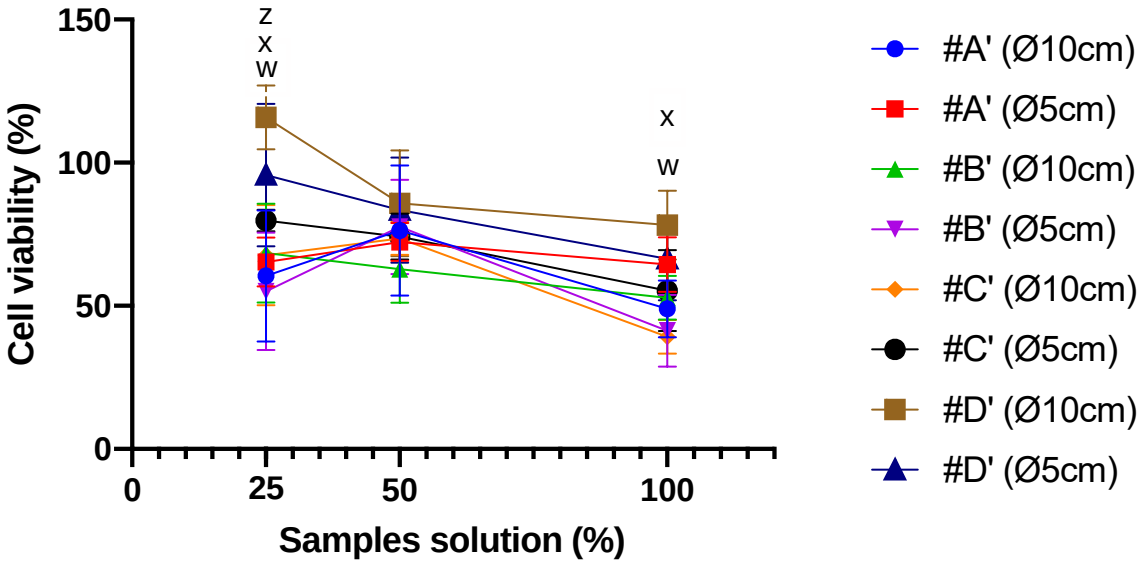

Figure 20 - Cell viability of MG63 when in contact with extracts of samples A'-D' in 3 different concentrations (25%, 50% and 100%) after 3 days of incubation. Control was done in TCPS and considered to have cell viability of 100% estimated by MTT assay. Statistically significant difference at 25% between samples: #A' (Ø10cm) and #D' (Ø5cm), and #C' (Ø5cm) and #D' (Ø10cm) (w - $p<0.05$); #D' (Ø10cm) and #A' (Ø5cm), #B' (Ø10cm) and #C' (Ø10cm) (y - $p<0.001$); #D' (Ø10cm) and both #A' (Ø10cm) and #B' (Ø5cm) (z - $p<0.0001$). Statistically significant difference at 100% between samples: #B' (Ø5cm) and #D' (Ø10cm) (w - $p<0.05$); #C' (Ø10cm) and #D' (Ø10cm) (x - $p<0.01$).

When comparing all the results (Fig. 13 to 20), it could be inferred that both L929 and MG63 cell line had a reduction of cellular viability along the time in most of the analysed samples. Another biocompatibility test was performed (Resazurin assay) to observe the direct effect of the materials on cellular behaviour. If we compare cell viability results of L929 and MG63 in indirect contact with materials A-D, we can observe that they are very similar. Furthermore, when analysing both cell types viability results in indirect contact with batches A'-D', it is possible to see that osteoblast-like cells showed higher viability when compared to fibroblasts. Thus, MG63 cellular viability was mainly promoted in the samples that undergo gamma irradiation. Therefore, L929 fibroblasts showed similar cellular viability in samples that were and were not irradiated.

Studies carried out by Laranjeira et. Al (2010), showed a cell viability of 100% on MG63 cells cultured for 3 days on nanoHA aggregates, which were higher cell viability values when compared to the results showed in this work.

After 6 days of incubation, there was as increase in cell viability (Laranjeira et al., 2010). The higher results should be related to the materials composition, since in these studies, unlike ours, the nanoHA was sintered and not dispersed, which is more stable and has lower degradation rate.

4.2.2 Resazurin assay

The resazurin assay is a test used to infer the cell viability through its metabolic activity. Resazurin is a non-fluorescent dye that is reduced in living cells by mitochondrial enzymes to resorufin, a fluorescent dye (Anoopkumar-Dukie et al., 2005).

In this work, the resazurin assay was performed to study the direct cytotoxicity of the samples when cultured with L929 and MG63 cells.

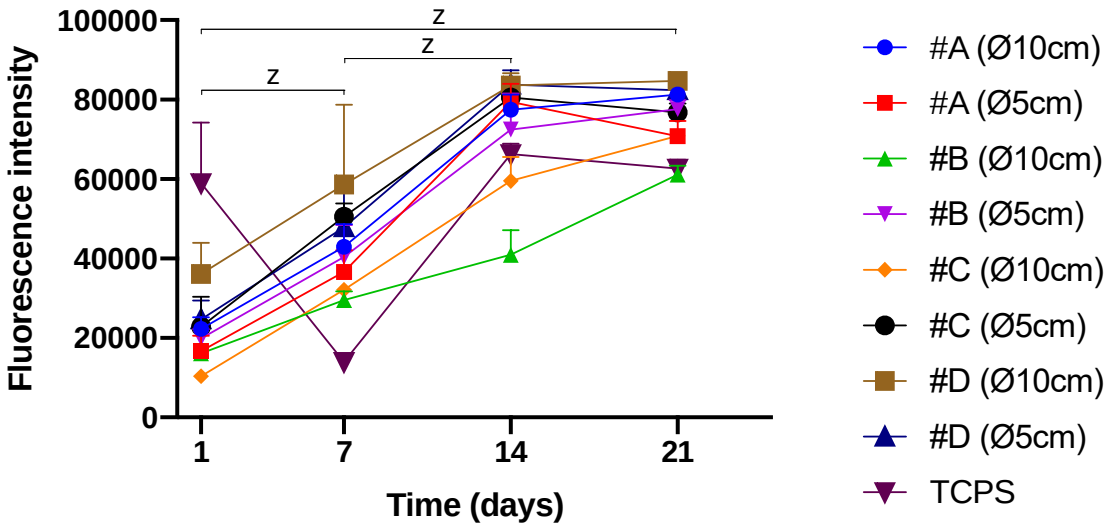

Figure 21 - Fluorescence intensity of L929 when in direct contact with samples A-D after 1, 7, 14 and 21 days of incubation estimated by Resazurin assay. Control was done in TCPS and considered to have cell viability of 100%. Statistically significant difference within the same sample for all the materials between day 1 and 7, day 7 and 14 and day 1 and 21 (z - $p<0.0001$).

Figure 21 represents the fluorescence intensity of L929 that were cultured into the materials A-D for 1, 7, 14 and 21 days. A higher fluorescence intensity is related to a higher metabolic activity and thus a higher cell viability.

It is possible to observe that cell viability increased until day 14, when it reached the highest values. After 21 days, cellular viability was very similar to day 14 in all the evaluated materials. The cells cultured into scaffolds D (Ø 10 cm and Ø 5 cm) showed higher cellular viability during the 3 week observation. All the tested materials showed significant higher metabolic activity from day 1 until day 21 when compared to the cells that were growing on TCPS (2D). This higher cell number could be related to a higher cell adhesion and proliferation at the materials surface.

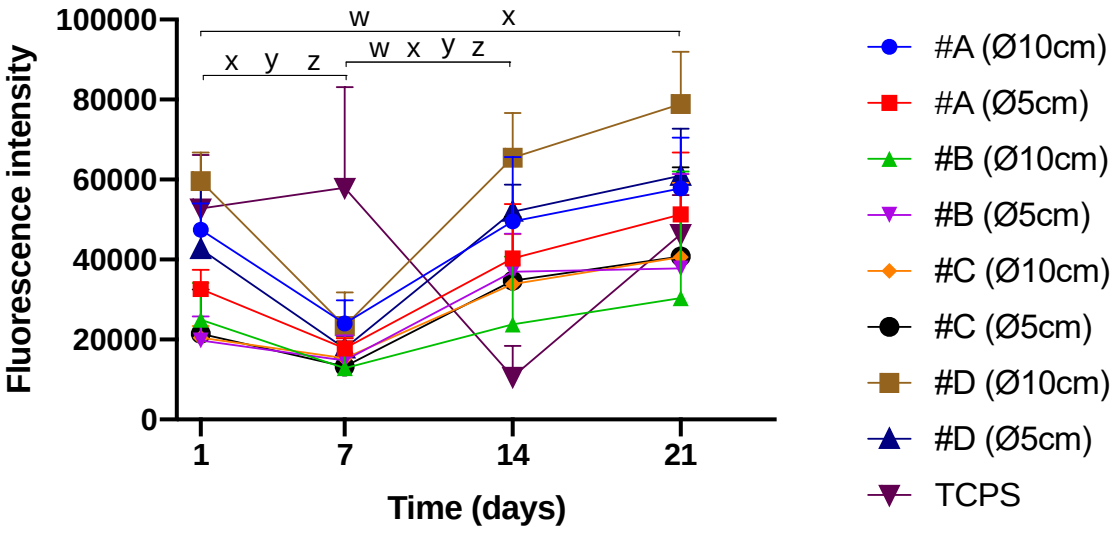

Figure 22 - Fluorescence intensity of MG63 when in direct contact with samples A-D after 1, 7, 14 and 21 days of incubation estimated by Resazurin assay. Control was done in TCPS and considered to have cell viability of 100%. Statistically significant difference between day 1 and 7 for samples #A (Ø10cm) (x - $p<0.01$), #D (Ø5cm) (y- $p<0.001$) and #D (Ø10cm) (z - $p<0.0001$). Statistically significant difference between day 7 and 14 for samples: #C (Ø10cm) (w - $p<0.05$); #A (Ø5cm), #B (Ø5cm) and #C (Ø5cm) (x - $p<0.01$); #A (Ø10cm) (y - $p<0.001$); #D (Ø10cm and Ø5cm) and TCPS (z - $p<0.0001$). Statistically significant difference between day 1 and 21 for samples: #A (Ø5cm), #B (Ø5cm), #C (Ø5cm) and #D (Ø10cm and Ø5cm) (w - $p<0.05$); #C (Ø10cm) (x - $p<0.01$).

The fluorescence intensity of osteoblast-like cells (MG63) cultured in direct contact with samples A-D through 3 weeks is presented in Figure 22.

During the first week the cellular viability of the MG63 cells was lower when compared to day 1 results. On day 14, cell viability increased and remained similar until the last observed time point (21 days). Scaffolds D (Ø 10 cm and Ø 5 cm) and A (Ø 10 cm and Ø 5 cm) showed higher cellular viability results with this cell culture in all time-points. All the tested samples showed an increase in cell viability from day 1 to day 21. This increase on the metabolic activity was significant in all the samples with the exception of materials A and B, both with Ø 10 cm.

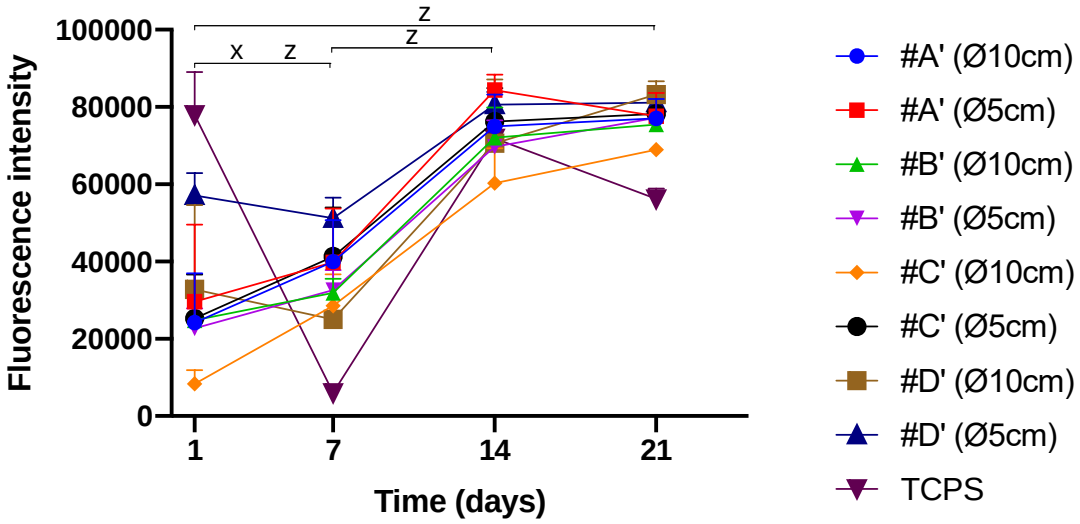

Figure 23 - Fluorescence intensity of L929 when in direct contact with samples A'-D' after 1, 7, 14 and 21 days of incubation estimated by Resazurin assay. Control was done in TCPS and considered to have cell viability of 100%. Statistically significant difference between day 1 and 7 for samples: #A' (Ø10cm) and #C' (Ø5cm) (x - $p<0.01$); #C' (Ø10cm) and TCPS (z - $p<0.0001$). Statistically significant difference between day 7 and 14 and between day 1 and 21 for all the tested materials (z - $p<0.0001$).

Figure 23 shows fluorescence intensity in correlation to the metabolic activity of fibroblasts (L929) when cultured into scaffolds A'-D' for 1, 7, 14 and 21 days.

Similarly to the results obtained with L929 in contact with samples A-D,

all the irradiated materials (A'-D') showed higher metabolic activity after 14 days of culture when compared to control results. On day 21, the observed metabolic activity results were very similar for all studied samples. It is also possible to observe that the materials A' with Ø 5 cm and D' with Ø 5 cm showed higher fibroblast metabolic activity, similar to the cell viability results observed from the non-irradiated tested samples. From day 1 until the end of the study, there was a statistical significant increase in cell viability for all the samples (A'-D', $p<0.0001$).

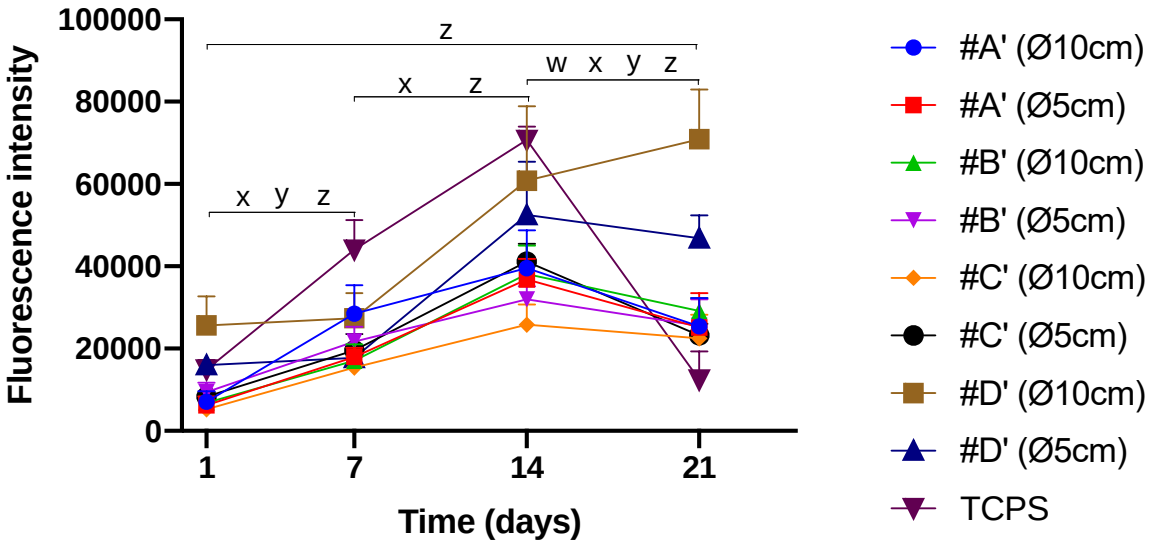

Figure 24 - Fluorescence intensity of MG63 when in direct contact of samples A'-D' after 1, 7, 14 and 21 days of incubation estimated by Resazurin assay. Control was done in TCPS and considered to have cell viability of 100%. Statistically significant difference between day 1 and 7 for samples: #B' (Ø10cm) and #C' (Ø10cm) (x - $p<0.01$); #A' (Ø5cm), #B' (Ø5cm) and #C' (Ø5cm) (y - $p<0.001$); #A' (Ø10cm) and TCPS (z - $p<0.0001$). Statistically significant difference between day 7 and 14 for samples: #A' (Ø10cm), #B' (Ø5cm), #C' (Ø10cm) (x - $p<0.01$); for the rest of the samples (z - $p<0.0001$). Statistically significant difference between day 14 and 21: #B' (Ø10cm) (w); #D' (Ø10cm) (x - $p<0.01$); #A' (Ø5cm) (y - $p<0.001$); #A' (Ø10cm), #C' (Ø5cm) and TCPS (z - $p<0.0001$). Statistically significant difference between day 1 and 21 for all the materials (z $p<0.0001$).

Finally, the fluorescence intensity of MG63 in direct contact with materials A' to D' is shown in Figure 24.

Until day 14, cells showed an increase in cell metabolic activity, followed by a significant decrease on day 21 in samples A' (Ø 10 cm and Ø 5 cm), B' (Ø 10 cm) and C' (Ø 5 cm). The samples from batch D' (Ø 10 cm and Ø 5 cm) showed higher cell viability after 21 days when compared to all the tested materials. From day 1 to day 21 there was a statistically significant increase in cell viability for all the studied samples (A'-D', $p<0.0001$).

Comparing the results of figures 21 to 24, it could be observed that fibroblasts had higher metabolic activity in materials A, D, A' and D' during the evaluated period of time and showed similar values for both irradiated and non-irradiated samples. Batches A and D, both with Ø 10 cm and Ø 5 cm showed higher fibroblast viability after 2 weeks of incubation. MG63 showed similar metabolic activity when cultured into all the tested materials. In both cell lines, the highest cellular viability was also observed on day 14 for samples of batch D (Ø 10 cm and Ø 5 cm) before and after irradiation. The increase in the metabolic activity showed in all the tested materials in comparison to the control should be related to the area available for the cell culture expansion, since the scaffolds had a 3D structure instead of 2D of the well-plates.

In previous studies, when compared to the control 2D, the results of MG63 metabolic activity within the scaffolds of collagen/nanoHA 50:50 % wt were of approximately 130% for day 1 and 150% for day 7 (C. et al., 2013). In contrast, our studies with osteoblast-like cells have showed lower cell viability in the same time points, but higher cell metabolic activity on day 21. In studies by Laranjeira et al. (2010), in which nanoHA aggregates were used, there was also an increase in fluoresce intensity from day 3 to day 6 (Laranjeira et al., 2010).

4.2.3 Alkaline phosphatase (ALP) activity

The assessment of the alkaline phosphatase activity was evaluated with osteoblast-like cells (MG63) after 14 and 21 days of culture within materials that were and were not gamma irradiated.

ALP is a parameter of early cell differentiation and, therefore, an indicator of the expression of the osteoblastic phenotype (Ren, Tsuru,

Hayakawa, & Osaka, 2002).

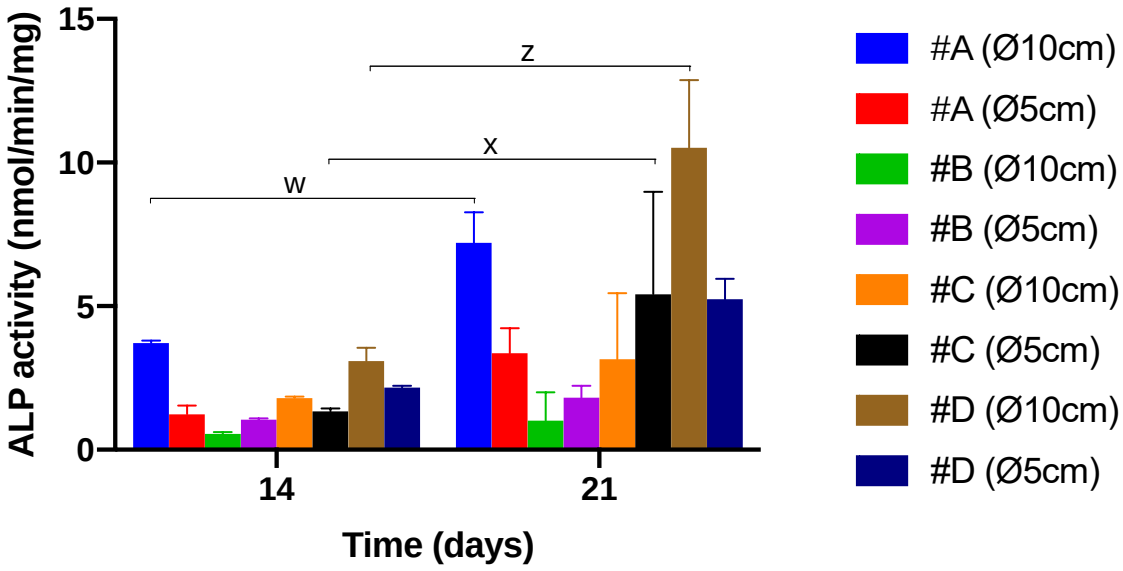

Figure 25 - ALP activity for osteoblastic phenotype expression of MG63 cultured within samples A-D for 14 and 21 days. Statistically significant difference between days 14 and 21 for samples #A (Ø10cm) (w - $p<0.05$), #C (Ø5cm) (x - $p<0.01$) and #D (Ø10cm) (z - $p<0.0001$).

Figure 25 shows the ALP activity of human osteoblast-like cells that were cultured into the materials that did not undergo irradiation.

As shown in this graph, the ALP activity was higher on day 21 when compared to day 14, especially for samples D and A, both with Ø 10 cm, and sample C with Ø 5 cm. This higher activity can be related to a higher nanoHA content for these samples, since this ceramic had been demonstrated to have influence on the enhancement of ALP activity of MG63 cells (Dvorak & Riccardi, 2004; Sugimoto et al., 1993; Tsai, Hsu, & Chen, 2008).

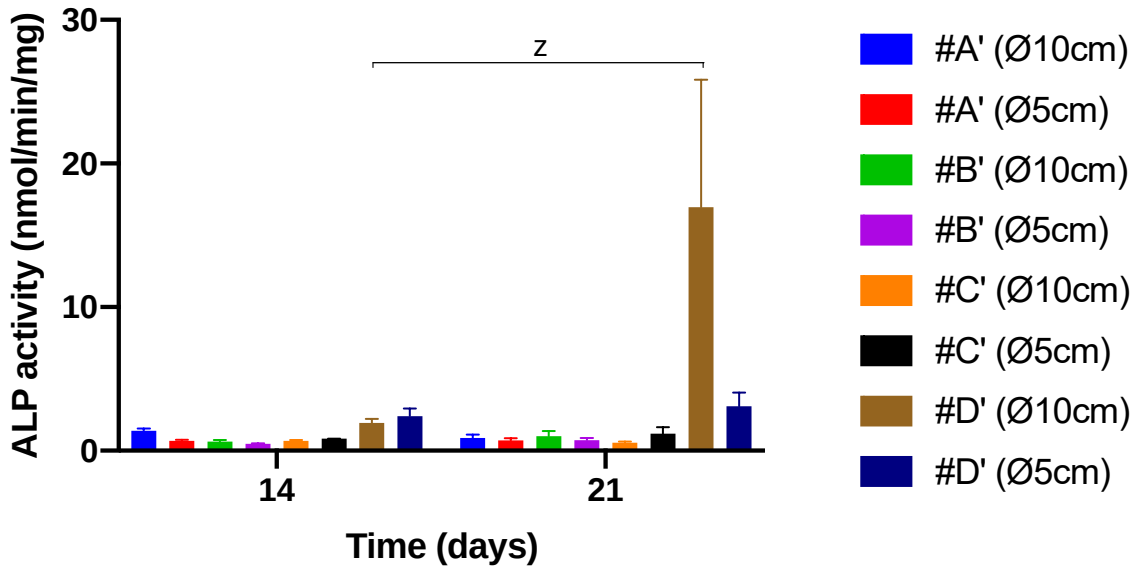

Figure 26 - ALP activity for osteoblastic phenotype expression of MG63 cultured within samples A'-D' for 14 and 21 days. Statistically significant difference between days 14 and 21 for sample #D' (Ø10cm) (z - $p<0.0001$).

The ALP activity in MG63 cells cultured into scaffolds A'-D' (irradiated samples) is shown in figure 26.

For all the materials B' and D', there was an increase in ALP activity from day 14 to day 21, but cells cultured onto scaffold D with Ø 10 cm showed higher ALP results and a statistically significant difference between the two time-points. It was possible to observe a decrease of the ALP activity results with materials A' and C' (both with Ø 10 cm) from day 14 to day 21, although not statistically significant. The ALP activity suffered a reduction probably due to the fact that cells reached a maximum confluence (Dong et al., 2009; H. Liu et al., 2005; Noda & Rodan, 1986), which might have occurred until day 14. In accordance with the results of samples without gamma irradiation, the larger membranes (Ø 10 cm), with the exception of batch C', showed higher ALP activity.

Comparing the ALP activity results of both graphs, it is possible to observe that scaffold D (Ø 10 cm) showed higher ALP activity after being irradiated. Similar effect was not shown on the other scaffolds batches (A-C), which showed higher ALP activity results when not irradiated. This should be associated to the gamma irradiation process, in which the energy produced by the sterilization method could promote some chemical alterations in the

polymer chains surface and could affect the cellular response.

In results observed in similar studies, the values for cells ALP activity cultured in scaffolds of collagen/nanoHA 50:50 % wt were 0.35 nmol/min/µg and 0.2 nmol/min/µg for cell culture time of 14 and 21 days, respectively (C. et al., 2013). Previous studies by Laranjeira et al. (2010) showed an increase in ALP activity from day 3 to day 6 for cells seeded in nanoHA granules (Laranjeira et al., 2010).

The ALP activity results for MG63 culture in both graphs (Fig. 24 and 25) showed higher enzyme activity when compared to values in studies conducted with similar biomaterials (C. et al., 2013; Laranjeira et al., 2010), as well as an increase in the ALP activity along the cell culture time.

4.2.4 DNA quantification assay

The PicoGreen assay was performed to quantify the amount of cellular DNA present in the samples (A-D and A'-D') and to study, over time, the proliferation rate of osteoblastic-like cells (MG63) after 14 and 21 days of culture in the scaffolds.

The quantification of cellular DNA in materials A-D after MG63 culture is presented in Figure 27.

In Figure 27, the highest concentration of cellular DNA could be observed on day 21, although in some samples it was observed a not statistical significant decrease in this concentration after 21 days (batches B and C). These decrease in cell number were similar to the results of lower cell metabolic activity observed in the Resazurin assay from day 14 to day 21 (Fig. 22 and 24). Batch A with Ø 10 cm showed a significant increase of the cellular DNA concentration after 21 days.

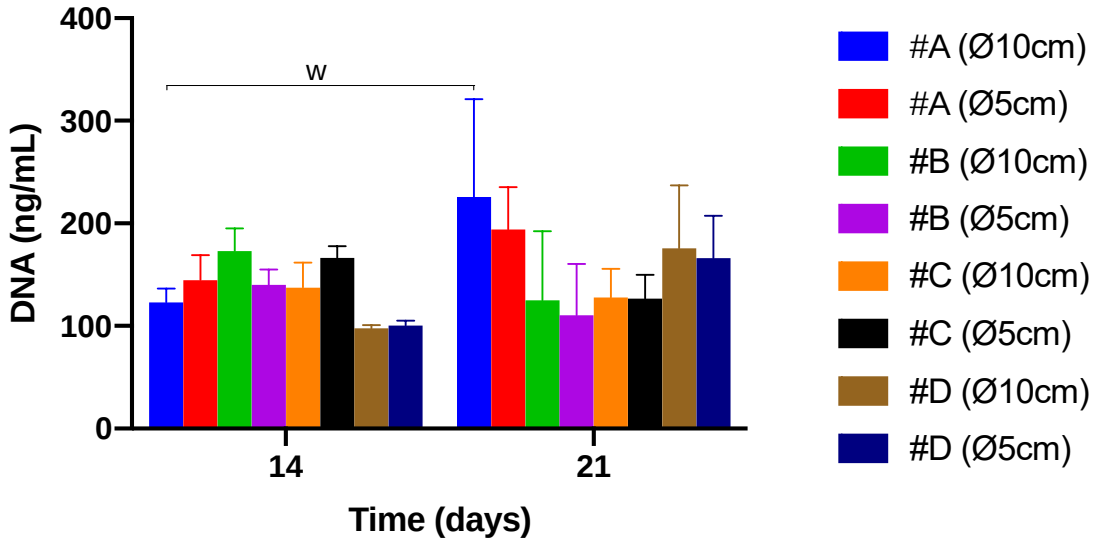

Figure 27 - Total DNA extraction quantification of MG63 cells cultured into samples A-D for 14 and 21 days. Statistically significant difference between days 14 and 21 for sample #A (Ø10cm) (w - $p<0.05$).

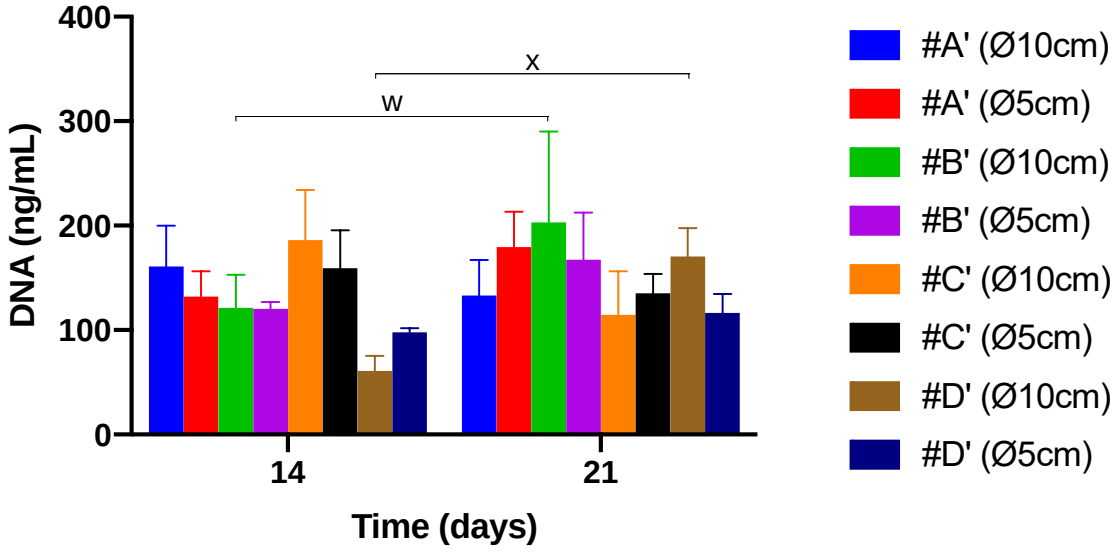

Figure 28 - Total DNA extraction quantification of MG63 cells cultured into samples A'-D' for 14 and 21 days. Statistically significant different between days 14 and 21 for samples #B' (Ø10cm) (w - $p<0.05$) and #D' (Ø10cm) (x - $p<0.01$).

Figure 28 shows the DNA quantification for cells in direct contact with materials that were gamma irradiated for sterilization.

The results showed higher cell DNA concentration from day 14 to day 21, in accordance to the results showed in Figure 26, except for batch C and A (Ø 10 cm). These two materials showed a decrease in cell number, though not statistically significant. The increase in DNA concentration was statistically significant for samples B' and D', both with Ø 10 cm after 21 days. These findings corroborated to the higher cellular metabolic activity results in the same materials (Resazurin assay - Fig. 22 and 24), where the cells showed a higher increase in cellular metabolic activity from 14 to 21 days.

Comparing the results from figures 27 and 28, the concentration of cellular DNA is similar for all smaller samples (Ø 5 cm) incubated for 14 days. However, the irradiated samples B' and D', both with Ø 5 cm showed higher and lower DNA concentration, respectively, after 21 days. The differences found between the different batches may be the result of a different topography of the cryogels with higher nanoHA aggregates on the surface of the materials as observed in the SEM images (Fig. 10). Rougher surfaces promote a higher proliferation rate of osteoblast-like cells when compared to smoother ones (Deligianni, Katsala, Koutsoukos, & Missirlis, 2000; Osathanon, Bespinyowong, Arksornnukit, Takahashi, & Pavasant, 2011; Ribeiro, Sousa, & Monteiro, 2010; Webster et al., 2000; Webster, Siegel, & Bizios, 1999).

In the studies performed by Sandra C. Rodrigues, cryogels of collagen-nanoHA 50:50 % wt cultured with MG63 cells showed DNA concentration of 50 ng/mL and 45 ng/mL after 14 and 21 days, respectively (C. et al., 2013). Therefore, considering the similarity of the published results and the figures showed in this work, we could infer that the osteoblastic-like cells behaviour should be influenced by the materials characteristics, favouring the cellular proliferation rate (Fig. 25 and 26).

4.2.4 Confocal laser scanning microscopy

Confocal laser scanning microscopy (CLSM) was used to study the morphology of MG63 cells after 21 days of culture within samples that have and have not been gamma irradiated.

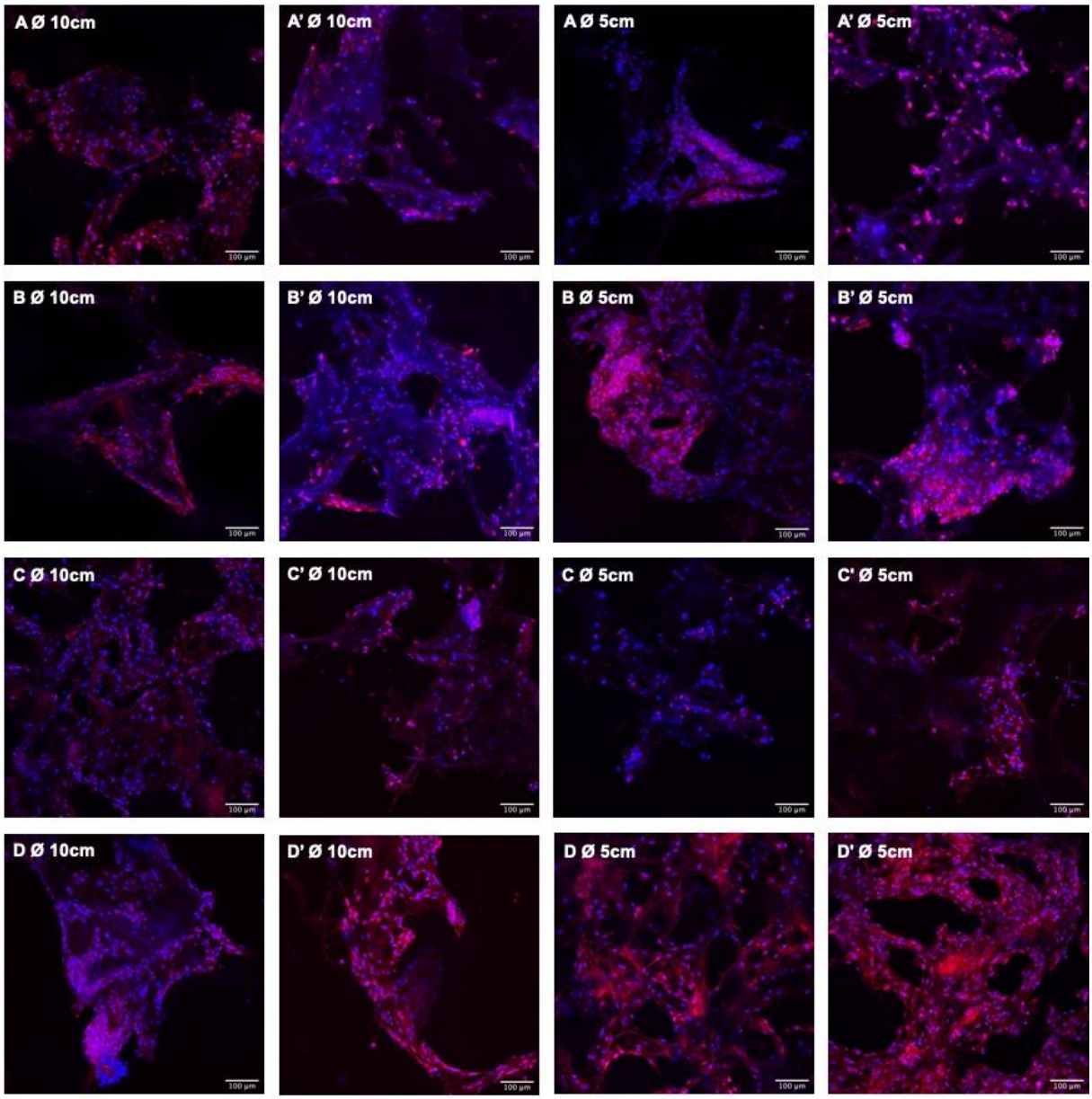

Figure 29 - CLSM images of MG63 cultured for 21 days on scaffolds A-D and A'-D'. Scale bar: 100 µm.

In figure 29, it is possible to observe the cellular morphology of osteoblast-like cells on cryogels surface with and without irradiation after 21 days incubation.

CLSM images show that the cells had adhered to the scaffolds' surface (proximally 100 µm deep), it was not possible to observe cells in the inner part of the scaffolds (over 150 µm), and in some samples, cells were detected only at the edges of the material. It was also possible to distinguish cells in two

different morphologies: one round and agglomerated and another spread and well adherent. Comparing cryogels A-D with A'-D', in the later ones it was possible to observe higher cell number for most of the samples (batches A, B and D). These observations are in accordance with the DNA quantification results (Fig. 27 and 28) that showed an increase in cell number after scaffolds irradiation. The lower number of cells in some samples (batch C) might be derived from the staining protocol that leads to many washing steps for CLSM analysis and could have promoted cell loss.

Chapter 5

Conclusion remarks and Future Perspectives

This work had as main objective the evaluation of a scale-up productive process for the development of a biomaterial based on collagen and nanohydroxyapatite at industrial prototype level. The work included the evaluation of the materials safety and reproducibility, in order to be used as a medical device in the orthopaedic area.

The tests performed for the physical characterization of the material, showed an ability of the scaffolds to absorb and retain solvents as well as adequate mechanical resistance and viscoelastic properties. The cryogels had a heteroporous morphology with microporosity and macroporosity, which are essential conditions for the interaction between the cells and materials and consequently promote bone regeneration.

Regarding the biological studies, all studied cryogels were non-cytotoxic for fibroblasts and osteoblast-like cells that were in direct or indirect contact with them. In fact, the scaffolds promoted the proliferation of the cells as well as promoting the expression of the osteoblastic phenotype (MG63 cell line).

In this work, no significant differences were observed between the larger (Ø 10 cm) and smaller (Ø 5 cm) membranes, or between the gamma irradiated and non-irradiated materials.

Before and after irradiation, all the studied scaffolds batches showed

considerable differences between them, which makes us conclude that the materials production process needs to be further optimised in order to become more reproducible.

As future work, *in vivo* studies are necessary in order to validate the *in vitro* results shown in this work. In a laboratory perspective, it would also be interesting to study the behaviour of the cells when in contact with materials modified with biological cues, such as, growth factors (i.e. bone morphogenic proteins, fibroblast growth factors or vascular endothelium growth factors) to better mimic the *in vivo* system. At the industrial level the next steps are the product certification by ISO and CE mark and also clinical trials for the product validation.

References

and, S. W., & Wagner, H. D. (1998). THE MATERIAL BONE: Structure-Mechanical Function Relations. *Annual Review of Materials Science, 28*(1), 271-298. doi:10.1146/annurev.matsci.28.1.271

Anoopkumar-Dukie, S., Carey, J. B., Conere, T., O'Sullivan, E., van Pelt, F. N., & Allshire, A. (2005). Resazurin assay of radiation response in cultured cells. *The British Journal of Radiology, 78*(934), 945-947. doi:10.1259/bjr/54004230

Bencherif, S., Warren Sands, R., Bhatta, D., Arany, P., Verbeke, C., A Edwards, D., & J Mooney, D. (2012). *Injectable preformed scaffolds with shape-memory properties* (Vol. 109).

Boskey, A. L. (2008). Osteoporosis and Osteopetrosis. In *Handbook of Biomineralization* (pp. 59-79).

Bowes, J. H., & Moss, J. A. (1962). The Effect of Gamma Radiation on Collagen. *Radiation Research, 16*(3), 211-223. doi:10.2307/3571153

Bran, G. M., Stern-Straeter, J., Hörmann, K., Riedel, F., & Goessler, U. R. (2008). Apoptosis in Bone for Tissue Engineering. *Archives of Medical Research, 39*(5), 467-482. doi:10.1016/j.arcmed.2008.02.007

C., R. S., L., S. C., Abhishek, S., P., G. M., H., F. M., & J., M. F. (2013). Preparation and characterization of collagen-nanohydroxyapatite biocomposite scaffolds by cryogelation method for bone tissue engineering applications. *Journal of Biomedical Materials Research Part A, 101A*(4), 1080-1094. doi:doi:10.1002/jbm.a.34394

Chang, M. C., & Tanaka, J. (2002). FT-IR study for hydroxyapatite/collagen nanocomposite cross-linked by glutaraldehyde. *Biomaterials, 23*(24), 4811-4818. doi:https://doi.org/10.1016/S0142-9612(02)00232-6

Clarke, B. (2008). Normal bone anatomy and physiology. *Clin J Am Soc Nephrol, 3 Suppl 3*, S131-139. doi:10.2215/cjn.04151206

Deligianni, D. D., Katsala, N. D., Koutsoukos, P. G., & Missirlis, Y. F. (2000). Effect of surface roughness of hydroxyapatite on human bone marrow cell adhesion, proliferation, differentiation and detachment strength. *Biomaterials, 22*(1), 87-96. doi:https://doi.org/10.1016/S0142-9612(00)00174-5

Dong, S.-W., Ying, D.-J., Duan, X.-J., Xie, Z., Yu, Z.-J., Zhu, C.-H., . . . Sun, J.-S. (2009). Bone Regeneration Using an Acellular Extracellular Matrix and Bone Marrow Mesenchymal Stem Cells Expressing Cbfa1. *Bioscience, Biotechnology, and Biochemistry, 73*(10), 2226-2233. doi:10.1271/bbb.90329

Du, C., Cui, F. Z., Feng, Q. L., Zhu, X. D., & de Groot, K. (1998). Tissue response to nano-hydroxyapatite/collagen composite implants in marrow cavity. *Journal of Biomedical Materials Research, 42*(4), 540-548. doi:10.1002/(SICI)1097-4636(19981215)42:4<540::AID-JBM9>3.0.CO;2-2

Dvorak, M. M., & Riccardi, D. (2004). Ca2+ as an extracellular signal in bone. *Cell Calcium, 35*(3), 249-255. doi:https://doi.org/10.1016/j.ceca.2003.10.014

Fierz, F. C., Beckmann, F., Huser, M., Irsen, S. H., Leukers, B., Witte, F., . . . Müller, B. (2008). The morphology of anisotropic 3D-printed hydroxyapatite scaffolds.

References

Biomaterials, 29(28), 3799-3806. doi:https://doi.org/10.1016/j.biomaterials.2008.06.012

Hixon, K. R., Eberlin, C. T., Kadakia, P. U., McBride-Gagyi, S. H., Jain, E., & Sell, S. A. (2016). A comparison of cryogel scaffolds to identify an appropriate structure for promoting bone regeneration. *Biomedical Physics and Engineering Express, 2*(3). doi:10.1088/2057-1976/2/3/035014

Hixon, K. R., Eberlin, C. T., Lu, T., Neal, S. M., Case, N. D., McBride-Gagyi, S. H., & Sell, S. A. (2017). The calcification potential of cryogel scaffolds incorporated with various forms of hydroxyapatite for bone regeneration. *Biomedical Materials (Bristol), 12*(2). doi:10.1088/1748-605X/aa5d76

Hixon, K. R., Lu, T., & Sell, S. A. (2017). A comprehensive review of cryogels and their roles in tissue engineering applications. *Acta Biomaterialia, 62*, 29-41. doi:10.1016/j.actbio.2017.08.033

Hixon, K. R., Melvin, A. M., Lin, A. Y., Hall, A. F., & Sell, S. A. (2017). Cryogel scaffolds from patient-specific 3D-printed molds for personalized tissue-engineered bone regeneration in pediatric cleft-craniofacial defects. *Journal of Biomaterials Applications, 32*(5), 598-611. doi:10.1177/0885328217734824

Hoffman, A. S. (2012). Hydrogels for biomedical applications. *Advanced Drug Delivery Reviews, 64*, 18-23. doi:https://doi.org/10.1016/j.addr.2012.09.010

Idaszek, J., Kijeńska, E., Łojkowski, M., & Swieszkowski, W. (2016). How important are scaffolds and their surface properties in regenerative medicine. *Applied Surface Science, 388*, 762-774. doi:https://doi.org/10.1016/j.apsusc.2016.03.038

Inzana, J. A., Olvera, D., Fuller, S. M., Kelly, J. P., Graeve, O. A., Schwarz, E. M., . . . Awad, H. A. (2014). 3D printing of composite calcium phosphate and collagen scaffolds for bone regeneration. *Biomaterials, 35*(13), 4026-4034. doi:https://doi.org/10.1016/j.biomaterials.2014.01.064

Jain, E., Srivastava, A., & Kumar, A. (2008). Macroporous interpenetrating cryogel network of poly(acrylonitrile) and gelatin for biomedical applications. *Journal of Materials Science: Materials in Medicine, 20*(1), 173. doi:10.1007/s10856-008-3504-4

Jiang, W., & Liu, H. (2016). 11 - Nanocomposites for bone repair and osteointegration with soft tissues. In H. Liu (Ed.), *Nanocomposites for Musculoskeletal Tissue Regeneration* (pp. 241-257). Oxford: Woodhead Publishing.

Jones, J. R., Gentleman, E., & Polak, J. (2007). Bioactive Glass Scaffolds for Bone Regeneration. *Elements, 3*(6), 393-399. doi:10.2113/GSELEMENTS.3.6.393

Kane, R. J., & Roeder, R. K. (2012). Effects of hydroxyapatite reinforcement on the architecture and mechanical properties of freeze-dried collagen scaffolds. *Journal of the Mechanical Behavior of Biomedical Materials, 7*, 41-49. doi:https://doi.org/10.1016/j.jmbbm.2011.09.010

Kathuria, N., Tripathi, A., Kar, K. K., & Kumar, A. (2009). Synthesis and characterization of elastic and macroporous chitosan–gelatin cryogels for tissue engineering. *Acta Biomaterialia, 5*(1), 406-418. doi:https://doi.org/10.1016/j.actbio.2008.07.009

Klenke, F. M., Liu, Y., Yuan, H., Hunziker, E. B., Siebenrock, K. A., & Hofstetter, W. (2008). Impact of pore size on the vascularization and osseointegration of ceramic bone substitutes in vivo. *Journal of Biomedical Materials Research Part A, 85A*(3), 777-786. doi:10.1002/jbm.a.31559

Laranjeira, M. S., Fernandes, M. H., & Monteiro, F. J. (2010). Innovative macroporous granules of nanostructured-hydroxyapatite agglomerates: Bioactivity and osteoblast-like cell behaviour. *Journal of Biomedical Materials Research Part A, 95A*(3), 891-900. doi:10.1002/jbm.a.32916

Laranjo, S. C., Liliana, G., Helena, F. M., Jorge, C. B., & Jorge, M. F. (2016). Biodegradation, biocompatibility, and osteoconduction evaluation of collagen-nanohydroxyapatite cryogels for bone tissue regeneration. *Journal of Biomedical Materials Research Part A, 104*(1), 57-70. doi:doi:10.1002/jbm.a.35540

Lazner, F., Gowen, M., Pavasovic, D., & Kola, I. (1999). Osteopetrosis and Osteoporosis: Two Sides of the Same Coin. *Human Molecular Genetics, 8*(10), 1839-1846. doi:10.1093/hmg/8.10.1839

Lee, C. H., Singla, A., & Lee, Y. (2001). Biomedical applications of collagen. *International Journal of Pharmaceutics, 221*(1), 1-22. doi:https://doi.org/10.1016/S0378-5173(01)00691-3

Leontiou, I., Matthopoulos, D. P., Tzaphlidou, M., & Glaros, D. (1993). The effect of gamma irradiation on collagen fibril structure. *Micron, 24*(1), 13-16. doi:https://doi.org/10.1016/0968-4328(93)90010-X

Lima, P. A. L., Resende, C. X., de Almeida Soares, G. D., Anselme, K., & Almeida, L. E. (2013). Preparation, characterization and biological test of 3D-scaffolds based on chitosan, fibroin and hydroxyapatite for bone tissue engineering. *Materials Science and Engineering: C, 33*(6), 3389-3395. doi:https://doi.org/10.1016/j.msec.2013.04.026

Liu, B., Harrell, R., Davis, R. H., Dresden, M. H., & Spira, M. (1989). The effect of gamma irradiation on injectable human amnion collagen. *Journal of Biomedical Materials Research, 23*(8), 833-844. doi:10.1002/jbm.820230803

Liu, H., Li, W., Shi, S., Habelitz, S., Gao, C., & DenBesten, P. (2005). MEPE is downregulated as dental pulp stem cells differentiate. *Archives of Oral Biology, 50*(11), 923-928. doi:https://doi.org/10.1016/j.archoralbio.2005.03.003

Lukashev, M. E., & Werb, Z. (1998). ECM signalling: orchestrating cell behaviour and misbehaviour. *Trends in Cell Biology, 8*(11), 437-441. doi:https://doi.org/10.1016/S0962-8924(98)01362-2

MedicalExpo. (2019). Bone substitutes. Retrieved from https://www.medicalexpo.com/medical-manufacturer/bone-substitute-10110.html

Muschler, G. F., Raut, V. P., Patterson, T. E., Wenke, J. C., & Hollinger, J. O. (2010). The Design and Use of Animal Models for Translational Research in Bone Tissue Engineering and Regenerative Medicine. *Tissue Engineering Part B: Reviews, 16*(1), 123-145. doi:10.1089/ten.teb.2009.0658

Nieto-Suárez, M., López-Quintela, M. A., & Lazzari, M. (2016). Preparation and characterization of crosslinked chitosan/gelatin scaffolds by ice segregation induced self-assembly. *Carbohydrate Polymers, 141*, 175-183. doi:https://doi.org/10.1016/j.carbpol.2015.12.064

Noda, M., & Rodan, G. A. (1986). Type-ß transforming growth factor inhibits proliferation and expression of alkaline phosphatase in murine osteoblast-like cells. *Biochemical and Biophysical Research Communications, 140*(1), 56-65. doi:https://doi.org/10.1016/0006-291X(86)91057-0

Osathanon, T., Bespinyowong, K., Arksornnukit, M., Takahashi, H., & Pavasant, P. (2011). Human osteoblast-like cell spreading and proliferation on Ti-6Al-7Nb surfaces of varying roughness. *Journal of Oral Science, 53*(1), 23-30. doi:10.2334/josnusd.53.23

Ott, S. M. (2018). Cortical or Trabecular Bone: What's the Difference? *American Journal of Nephrology, 47*(6), 373-375. doi:10.1159/000489672

Patravale, V., Dandekar, P., & Jain, R. (2012). 4 - Nanotoxicology: evaluating toxicity potential of drug-nanoparticles. In V. Patravale, P. Dandekar, & R. Jain (Eds.), *Nanoparticulate Drug Delivery* (pp. 123-155): Woodhead Publishing.

Petite, H., Viateau, V., Bensaïd, W., Meunier, A., de Pollak, C., Bourguignon, M., . . . Guillemin, G. (2000). Tissue-engineered bone regeneration. *Nature Biotechnology, 18*(9), 959-963. doi:10.1038/79449

Raina, D. B., Isaksson, H., Teotia, A. K., Lidgren, L., Tägil, M., & Kumar, A. (2016). Biocomposite macroporous cryogels as potential carrier scaffolds for bone active agents augmenting bone regeneration. *Journal of Controlled Release, 235*, 365-378. doi:https://doi.org/10.1016/j.jconrel.2016.05.061

Razavi, M., Qiao, Y., & Thakor, A. S. (2019). Three-dimensional cryogels for biomedical applications. *Journal of Biomedical Materials Research Part A, 0*(0). doi:10.1002/jbm.a.36777

Ren, L., Tsuru, K., Hayakawa, S., & Osaka, A. (2002). Novel approach to fabricate porous gelatin–siloxane hybrids for bone tissue engineering. *Biomaterials, 23*(24), 4765-4773. doi:https://doi.org/10.1016/S0142-9612(02)00226-0

References

Rho, J.-Y., Kuhn-Spearing, L., & Zioupos, P. (1998). Mechanical properties and the hierarchical structure of bone. *Medical Engineering & Physics, 20*(2), 92-102. doi:https://doi.org/10.1016/S1350-4533(98)00007-1

Ribeiro, N., Sousa, S. R., & Monteiro, F. J. (2010). Influence of crystallite size of nanophased hydroxyapatite on fibronectin and osteonectin adsorption and on MC3T3-E1 osteoblast adhesion and morphology. *Journal of Colloid and Interface Science, 351*(2), 398-406. doi:https://doi.org/10.1016/j.jcis.2010.08.013

Riddle, R. C., & Clemens, T. L. (2017). Bone Cell Bioenergetics and Skeletal Energy Homeostasis. *Physiol Rev, 97*(2), 667-698. doi:10.1152/physrev.00022.2016

Ruchi, M., Kumar, G. S., Chand, G. K., & Ashok, K. (2014). Biocomposite Cryogels as Tissue-Engineered Biomaterials for Regeneration of Critical-Sized Cranial Bone Defects. *Tissue Engineering Part A, 20*(3-4), 751-762. doi:10.1089/ten.tea.2013.0072

Rücker, M., Laschke, M. W., Junker, D., Carvalho, C., Tavassol, F., Mülhaupt, R., . . . Menger, M. D. (2008). Vascularization and biocompatibility of scaffolds consisting of different calcium phosphate compounds. *Journal of Biomedical Materials Research Part A, 86A*(4), 1002-1011. doi:10.1002/jbm.a.31722

Seeley, R. R., Stephens, T. D., & Tate, P. (2002). *Essentials of anatomy and physiology*: McGraw-Hill.

Shakya, A. K., & Kandalam, U. (2017). Three-dimensional macroporous materials for tissue engineering of craniofacial bone. *British Journal of Oral and Maxillofacial Surgery, 55*(9), 875-891. doi:https://doi.org/10.1016/j.bjoms.2017.09.007

Shoulders, M. D., & Raines, R. T. (2009). Collagen Structure and Stability. *Annual Review of Biochemistry, 78*(1), 929-958. doi:10.1146/annurev.biochem.77.032207.120833

Singh, R., Lee, P. D., Lindley, T. C., Dashwood, R. J., Ferrie, E., & Imwinkelried, T. (2009). Characterization of the structure and permeability of titanium foams for spinal fusion devices. *Acta Biomaterialia, 5*(1), 477-487. doi:https://doi.org/10.1016/j.actbio.2008.06.014

Sionkowska, A. (2011). Current research on the blends of natural and synthetic polymers as new biomaterials: Review. *Progress in Polymer Science, 36*(9), 1254-1276. doi:https://doi.org/10.1016/j.progpolymsci.2011.05.003

Sionkowska, A., & Kozłowska, J. (2013). Properties and modification of porous 3-D collagen/hydroxyapatite composites. *International Journal of Biological Macromolecules, 52*, 250-259. doi:https://doi.org/10.1016/j.ijbiomac.2012.10.002

Sowjanya, J. A., Singh, J., Mohita, T., Sarvanan, S., Moorthi, A., Srinivasan, N., & Selvamurugan, N. (2013). Biocomposite scaffolds containing chitosan/alginate/nano-silica for bone tissue engineering. *Colloids and Surfaces B: Biointerfaces, 109*, 294-300. doi:https://doi.org/10.1016/j.colsurfb.2013.04.006

Stevens, M. M., & George, J. H. (2005). Exploring and Engineering the Cell Surface Interface. *Science, 310*(5751), 1135-1138. doi:10.1126/science.1106587

Suchanek, W., & Yoshimura, M. (1998). Processing and properties of hydroxyapatite-based biomaterials for use as hard tissue replacement implants. *Journal of Materials Research, 13*(1), 94-117. doi:10.1557/JMR.1998.0015

Sugimoto, T., Kanatani, M., Kano, J., Kaji, H., Tsukamoto, T., Yamaguchi, T., . . . Chihara, K. (1993). Effects of high calcium concentration on the functions and interactions of osteoblastic cells and monocytes and on the formation of osteoclast-like cells. *Journal of Bone and Mineral Research, 8*(12), 1445-1452. doi:10.1002/jbmr.5650081206

Tian, X. F., Heng, B. C., Ge, Z., Lu, K., Rufaihah, A. J., Fan, V. T. W., . . . Cao, T. (2008). Comparison of osteogenesis of human embryonic stem cells within 2D and 3D culture systems. *Scandinavian Journal of Clinical and Laboratory Investigation, 68*(1), 58-67. doi:10.1080/00365510701466416

Torres, F. G., Nazhat, S. N., Sheikh Md Fadzullah, S. H., Maquet, V., & Boccaccini, A. R. (2007). Mechanical properties and bioactivity of porous PLGA/TiO2 nanoparticle-filled composites for tissue engineering scaffolds. *Composites Science and Technology, 67*(6), 1139-1147. doi:https://doi.org/10.1016/j.compscitech.2006.05.018

Tsai, S.-W., Hsu, F.-Y., & Chen, P.-L. (2008). Beads of collagen–nanohydroxyapatite composites prepared by a biomimetic process and the effects of their surface texture on cellular behavior in MG63 osteoblast-like cells. *Acta Biomaterialia, 4*(5), 1332-1341. doi:https://doi.org/10.1016/j.actbio.2008.03.015

V., D. S., & Matthias, E. (2002). Biological and Medical Significance of Calcium Phosphates. *Angewandte Chemie International Edition, 41*(17), 3130-3146. doi:doi:10.1002/1521-3773(20020902)41:17<3130::AID-ANIE3130>3.0.CO;2-1

Walsh, J. S. (2015). Normal bone physiology, remodelling and its hormonal regulation. *Surgery (Oxford), 33*(1), 1-6. doi:https://doi.org/10.1016/j.mpsur.2014.10.010

Webster, T. J., Ergun, C., Doremus, R. H., Siegel, R. W., & Bizios, R. (2000). Specific proteins mediate enhanced osteoblast adhesion on nanophase ceramics. *Journal of Biomedical Materials Research, 51*(3), 475-483. doi:10.1002/1097-4636(20000905)51:3<475::AID-JBM23>3.0.CO;2-9

Webster, T. J., Siegel, R. W., & Bizios, R. (1999). Osteoblast adhesion on nanophase ceramics. *Biomaterials, 20*(13), 1221-1227. doi:https://doi.org/10.1016/S0142-9612(99)00020-4

Wei, J., Jia, J., Wu, F., Wei, S., Zhou, H., Zhang, H., . . . Liu, C. (2010). Hierarchically microporous/macroporous scaffold of magnesium–calcium phosphate for bone tissue regeneration. *Biomaterials, 31*(6), 1260-1269. doi:https://doi.org/10.1016/j.biomaterials.2009.11.005

Wu, X., Liu, Y., Li, X., Wen, P., Zhang, Y., Long, Y., . . . Gao, J. (2010). Preparation of aligned porous gelatin scaffolds by unidirectional freeze-drying method. *Acta Biomaterialia, 6*(3), 1167-1177. doi:https://doi.org/10.1016/j.actbio.2009.08.041

Yeong, W.-Y., Chua, C.-K., Leong, K.-F., Chandrasekaran, M., & Lee, M.-W. (2007). Comparison of drying methods in the fabrication of collagen scaffold via indirect rapid prototyping. *Journal of Biomedical Materials Research Part B: Applied Biomaterials, 82B*(1), 260-266. doi:10.1002/jbm.b.30729